Science of the Total Environment 947 (2024) 174409

Contents lists available at ScienceDirect

Science of the Total Environment

journal homepage: www.elsevier.com/locate/scitotenv

Effects of enzyme-induced carbonate precipitation technique on multiple heavy metals immobilization and unconfined compressive strength improvement of contaminated sand

Yi Bian [a], Yanbo Chen [a,b,*], Liangtong Zhan [a], Haowen Guo [c], Han Ke [a], Yuze Wang [d], Qingyang Wang [a], Yufeng Gao [e], Yunqi Gao [f]

[a] MOE Key Laboratory of Soft Soils and Geoenvironmental Engineering, Zhejiang University, Hangzhou, China
[b] Center for Hypergravity Experiment and Interdisciplinary Research, Zhejiang University, Hangzhou, China
[c] Guangzhou Institute of Energy Conversion, Chinese Academy of Sciences (CAS), Guangzhou 510640, PR China
[d] Department of Ocean Science and Engineering, Southern University of Science and Technology, Shenzhen 518055, China
[e] Key Laboratory of Ministry of Education for Geomechanics and Embankment Engineering, Hohai University, Nanjing, China
[f] Hebei University, No. 180 Wusi Dong Road, Lian Chi District, Baoding City, Hebei Province, China

HIGHLIGHTS

- Enzyme-induced carbonate precipitation method was applied for the heavy metal immobilization in contaminated sand.
- The immobilization percentage of Zn^{2+}, Ni^{2+} and Cr(VI) can be up to 99.9%, 86.38%, and 75.18%, respectively.
- Biomineralization, adsorption and complexation by organic molecules and $CaCO_3$ are immobilization mechanisms of EICP method.
- The unconfined compressive strength of EICP-treated contaminated sand specimens reached 306 kPa after four treatment cycles.

GRAPHICAL ABSTRACT

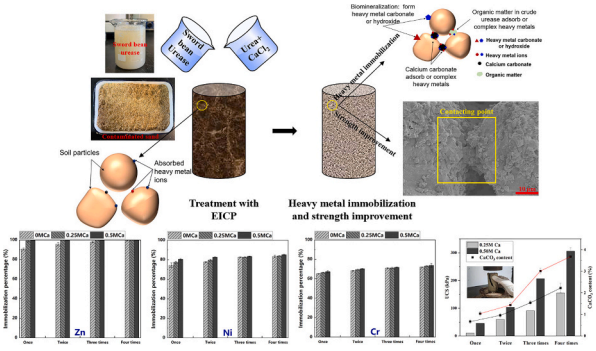

ARTICLE INFO

Editor: Bo Gao

Keywords:
Enzyme induced carbonate precipitation
Calcium carbonate
Urease activity
Heavy metal contamination
Plant-derived crude urease

ABSTRACT

Enzyme-induced carbonate precipitation (EICP) has been studied in remediation of heavy metal contaminated water or soil in recent years. This paper aims to investigate the immobilization mechanism of Zn^{2+}, Ni^{2+}, and Cr (VI) in contaminated sand, as well as strength enhancement of sand specimens by using EICP method with crude sword bean urease extracts. A series of liquid batch tests and artificially contaminated sand remediation experiments were conducted to explore the heavy metal immobilization efficacy and mechanisms. Results showed that the urea hydrolysis completion efficiency decreased as the Ca^{2+} concentration increased and the heavy metal immobilization percentage increased with the concentration of Ca^{2+} and treatment cycles in contaminated sand. After four treatment cycles with 0.5 mol/L Ca^{2+} added, the immobilization percentage of Zn^{2+}, Ni^{2+}, and Cr(VI) were 99.99 %, 86.38 %, and 75.18 %, respectively. The microscale analysis results presented that carbonate precipitates and metallic oxide such as $CaCO_3$, $ZnCO_3$, $NiCO_3$, $Zn(OH)_2$, and CrO(OH) were generated in

* Corresponding author at: MOE Key Laboratory of Soft Soils and Geoenvironmental Engineering, Zhejiang University, Hangzhou, China.
E-mail address: chenyanbo@zju.edu.cn (Y. Chen).

https://doi.org/10.1016/j.scitotenv.2024.174409
Received 3 February 2024; Received in revised form 18 June 2024; Accepted 29 June 2024
Available online 1 July 2024

liquid batch tests and sand remediation experiments. The SEM-EDS and FTIR results also showed that organic molecules and $CaCO_3$ may adsorb or complex heavy metal ions. Thus, the immobilization mechanism of EICP method with crude sword bean urease can be considered as biomineralization, as well as adsorption and complexation by organic matter and calcium carbonate. The unconfined compressive strength of EICP-treated contaminated sand specimens demonstrated a positive correlation with the increased generation of carbonate precipitates, being up to 306 kPa after four treatment cycles with shear failure mode. Crude sword bean urease with 0.5 mol/L Ca^{2+} added is recommended to immobilize multiple heavy metal ions and enhance soil strength.

1. Introduction

The issue of heavy metal contamination in water or soil from industrial resources, such as electronic industry, mine tailings, wastes disposal, waste water treatment sludge, and fuel consumption, has been a tough problem for a long time (Intawongse and Dean, 2006; Khan et al., 2021; Palansooriya et al., 2020; Ping et al., 2009). Studies have reported that the contaminated soils in tailings reservoir, industrial and municipal solid waste landfill can produce a large amount of heavy metal leachate under the influence of rainfall (Salleh and Hamid, 2013; Wang et al., 2024a). The toxic heavy metals (e.g., Zn^{2+}, Ni^{2+}, Cr(VI), Pb^{2+}, and Cd^{2+}) in leachate may leach into groundwater or surface water, posing potential threats to ecosystems and human health (Achal et al., 2011; Pruvot et al., 2006; Xu et al., 2021). In addition, the contaminated soils have been dumped into the landfill or tailings reservoir, thereby forming a large number of high slopes (Stark Timothy et al., 2000; Yu and Batlle, 2011; Zhan et al., 2023). Under the influence of rainfall infiltration, the buildup of water level can decrease the shear strength of contaminated soil, resulting in the instability and collapse of contaminated soil slopes (Feng et al., 2019; Huang and Fan, 2016; Guo et al., 2023). Koerner and Soong (2012) found that the triggering mechanisms for ten large landfill failures were the accumulation of pore water pressure and reduction in shear strength within the soil. Therefore, it is imperative to explore an effective method that can prevent the heavy metals from being leached out and improve soil shear strength.

Traditional methods used to remediate heavy metal contaminated soil including chemical precipitation, adsorption, soil washing, electrokinetics, and stabilization/solidification (S/S) have been extensively investigated in past decades (Dhami et al., 2017; Fu and Wang, 2011; Zhou et al., 2020). However, these chemical, physical methods are not only highly-cost, but also environmentally unfriendly, which inhibits the large-scale practical application (Hu et al., 2021a; Kang et al., 2016; Liu et al., 2021). Compared with conventional remediation technologies, biological method using microbial-induced carbonate precipitation (MICP) was considered as cost-effective and more efficient alternative, particularly for low-metal-contaminated water and soil (Krajewska, 2018; Qu et al., 2017; Li et al., 2023). This method was widely acknowledged for the ease of implementation and the absence of secondary pollution risks (Kang et al., 2015). So far, relevant research have found that heavy metal ions such as Cd^{2+}, Pb^{2+}, Cu^{2+}, and Zn^{2+} can be removed either by incorporation into calcite crystal lattice to form complex mineral precipitation (Hu et al., 2021a; Song et al., 2022) or by absorption of extracellular polymeric substances (EPS) (Kang et al., 2015; Tyagi et al., 2020; Zeng et al., 2021). However, studies have also reported that the heavy metals interference with the metabolism of the bacterial strains, thus retarding the bacteria growth (Sengor et al., 2009) and affecting urease secretion (Abdel-Gawwad et al., 2020). In addition, the applicability of MICP to fine-grained contaminated soil is also limited due to the constrained transport of bacteria (the diameter of bacterial cells is 5um) in pore-throat space (DeJong et al., 2010; Gao et al., 2019; Khodadadi et al., 2017).

Recently, enzyme-induced carbonate precipitation (EICP) has attracted great attention as a potential alternative to MICP for the heavy metal remediation in contaminated water or soil (Wang et al., 2022). EICP uses free urease enzyme as the catalyst and the size of urease molecules is about 7-10 nm (Erickson, 2009). The EICP process can be divided into two main steps. Firstly, urea is hydrolyzed into ammonia and carbonate ion through the catalytic capacity of urease. The majority of the ammonia remains in the formation of ammonium (NH_4^+) in water. Subsequently, the heavy metal cation or Ca^{2+} combine with carbonate ion to form heavy metal carbonate or calcium carbonate precipitates. Eqs. (1)–(4) show the chemical reactions involved in EICP process in aqueous solutions (Lai et al., 2023). It is worth mentioning that the effectively management of the by-product (e.g. ammonium chloride) is crucial, since it is a groundwater contaminant (Böhlke et al., 2006; Chang and Chung, 2000; Mao et al., 2018).

$$CO(NH_2)_2 + H_2O \xrightarrow{Urease\ enzyme} 2NH_3 + CO_2 \quad (1)$$

$$2NH_3 + 2H_2O \leftrightarrow 2NH_4^+ + 2OH^- \quad (2)$$

$$CO_2 + 2OH^- \leftrightarrow HCO_3^- + OH^- \leftrightarrow CO_3^{2-} + H_2O \quad (3)$$

$$Ca^{2+} + CO_3^{2-} \rightarrow CaCO_3 \quad (4)$$

Nam et al. (2016) used *Canavalia ensiformis* crude extracts to remediate heavy metal contaminated mine wastes, and the As, Mn, Zn, Pb, Cr, and Cu in leachates from the mine waste were effectively reduced. After that, non-fat milk was added into highly-purified commercial urease to deal with Cd, Pb, Ni contaminated soil and observed a better performance in heavy metal immobilization efficacy (Moghal et al., 2020). Moghal et al. (2023) found that EICP treatment improved the adsorption capacity of Cd, Ni, and Pb by contaminated soil, encapsulating heavy metals in soil with the order of Cd > Ni > Pb. Xie et al. (2024) have proposed incorporating nano-hydroxyapatite (nHAP) into the bioremediation process to enhance biomineralization efficacy. It was shown that nHAP can prevent the attachment of Pb^{2+} onto urease by (1) competing with urease, and (2) promoting Ca^{2+}/Pb^{2+} ion exchange. Recent research has focused on integrating EICP with chemical remediation methods to enhance the capacity for remediating heavy metal-contaminated soil. Wang et al. (2023a) introduced a modified electrokinetic reactor that incorporates the EICP into a permeable reactive barrier (PRB), significantly improve the removal efficiency of Pb^{2+} and Cu^{2+} in contaminated loess for about 4 times higher than before. Additionally, they found that the NH_4^+ recovery could reach up to 100 % with the addition of $MgCl_2$, and Na_2HPO_4 to the modified bio-PRB (Wang et al., 2023b). Furthermore, Wang et al. (2024b) demonstrated that struvite precipitation and ethylenediaminedisuccinic acid could mitigate NH_4^+ pollution and enhance the removal of Cu and Pb from contaminated loess using the bio-PRB technology. Although preceding studies have demonstrated the effectiveness of heavy metal immobilization by EICP using both highly-purified commercial urease and crude urease extracts, the underlying mechanism of how multiple heavy metals are immobilized, along with the interplay between heavy metal ions, calcium carbonate precipitates and organic molecules in crude urease extracts, still remains unclear.

So far, EICP technique has been widely applied to improve basic mechanical properties of sand, such as enhancing soil shear strength, reducing soil permeability and controlling dust (Cui et al., 2022; Chen et al., 2021a; Chen et al., 2021b; Chen et al., 2024; Gao et al., 2020, 2019; Wang et al., 2024). Among them, the shear strength is one of the most important properties of soil. It is the maximum magnitude of shear stress that soil can withstand (Hendry, 2018). Typically, the shear

strength is simply referred to as the strength of the soil. The Unconfined Compressive Test is the most widely used method for soil shear testing because it is both quick and cost-effective for measuring shear strength (Hossain et al., 2021). Hence, the Unconfined Compressive Strength (UCS) is commonly used to represent the mechanical properties and effectiveness of strength improvement in bio-cemented sand (Almajed et al., 2019; Xiao et al., 2023; Yao et al., 2021; Zhao et al., 2014). Kavazanjian and Hamdan (2015) used EICP method to reinforce sand columns and the peak Unconfined Compressive Strength after EICP treatment were 391–529 kPa. Martin et al. (2021) pointed out that the urease solution modified with powdered milk could result in enhanced unconfined compressive strength of sand columns. Studies also confirmed better effect of soil strength reinforcement with low cost when using crude urease extracts (Lai et al., 2024; Liu et al., 2023a; Miao et al., 2024; Nam et al., 2014). Nonetheless, to date, EICP with crude urease extracts was barely used for the dual purpose of heavy metal immobilization and strength enhancement for contaminated soil.

In this study, the immobilization efficacy and mechanism of Zn^{2+}, Ni^{2+}, and Cr(VI) in artificially contaminated sand, as well as strength enhancement of sand specimens were investigated by using EICP method with crude sword bean urease extracts. Firstly, in order to explore the heavy metal influence on pH, urea hydrolysis completion efficiency and Ca^{2+} immobilization percentage with time, which can help explain immobilization mechanism in contaminated sand, the liquid batch tests were conducted. The heavy metal immobilization percentage in liquid batch tests was also measured to provide reference for sand specimen experiments. Secondly, contaminated sand remediation experiments were carried out to explore heavy metal immobilization efficacy and mechanism of EICP method. Finally, the unconfined compressive strength of EICP-treated contaminated sand specimens were tested and the failure mode was discussed. Additionally, the micro-characterization of precipitates in both liquid batch tests and sand remediation experiments were observed to further provide insights into mechanisms for heavy metal immobilization by EICP method.

2. Materials and methods

2.1. Crude urease extracts preparation

The crude sword bean urease solutions were extracted from sword beans (*Canavalia gladiata* (Jacq.) DC., bought from commercial sources and grown in Guangxi province, China). In this study, the same procedures in Liu et al. (2023a) were used to extract urease: (a) the sword beans were grinded into fine powder, (b) the powder was mixed with deionized water to obtain a homogeneous suspension, (c) the suspension was centrifuged at 4 °C and 3000 r/min for 15 min and filtered. The clean supernatant liquids were kept as the crude sword bean urease extracts. The extracted supernatant liquid is rich in urease, an enzyme with catalytic properties that facilitates the hydrolysis of urea (Khodadadi Tirkolaei et al., 2020; Meng et al., 2021; Qi et al., 2022). The removal of remaining solid impurities through centrifugation and filtration is crucial to prevent surface clogging and ensuring the infiltration of the treatment solution in subsequent soil experiments (Liu et al., 2023a).

The urease property can be demonstrated by its activity, with higher activity resulting in a faster urea hydrolysis rate. Therefore, urease activity (abbreviated as UA) refers to the amount of the urea per minute that can be decomposed by sword bean urease (mmol/L/min). Electrical conductivity (EC) method was often used in previous studies to measure urease activity for its accuracy and convenience (Cui et al., 2022). Due to the interference with electrical conductivity results by heavy metal ions in solution, urease activity in this study was determined by ammonium production rate following the method proposed by Whiffin et al. (2007). The correlation between concentration and UA of sword bean urease in deionized water was shown in Supplemental file S1 (a). Before the subsequent liquid batch tests, some pre-tests were conducted to determine the concentration of sword bean urease in this study. In the pre-tests, the concentrations of urea and Zn^{2+}, Ni^{2+}, and Cr(VI) in solution were same with those used in the liquid batch tests (see Section 2.3), and three concentrations of sword bean urease (10 g/L, 15 g/L, and 20 g/L) were tested. The results in Supplemental file S1 (b) have shown that urease concentrations below 20 g/L quickly lost the catalytic activity in multiple heavy metal solution, resulting in the hydrolysis of only about 20 % of the urea. The final urea hydrolysis completion efficiency for using 20 g/L of sword bean urease could reach over 90 %. Therefore, the 20 g/L crude sword bean solution with 12 mmol/L/min of UA was used in both liquid batch tests and sand specimen experiments.

2.2. Contaminated sand specimen preparation

Chinese ISO Standard sand was used in this study and it was classified as well graded quartz sand according to Unified Soil Classification System (USCS) (ASTM 2007). Studies have reported that the particle size distribution of contaminated soil in landfills is similar with those of sand (Wickramarachchi et al., 2011; Zhang et al., 2017a). Supplemental file S2 illustrates the particle size distribution of the sand and the corresponding physical properties are shown in Supplemental file S3-Table. 1. The sand was thoroughly washed and kept clean before experiments.

The sand was artificially contaminated by Zn^{2+}, Ni^{2+}, and Cr(VI) using zinc chloride ($ZnCl_2$), nickel chloride ($NiCl_2$), and potassium dichromate ($K_2Cr_2O_7$) solution and the target concentration of each heavy metal in the sand was 50 mg/kg. The contaminated procedure was similar to Sharma et al. (2022): (a) Take some oven-dried sand with known mass; (b) Prepare $ZnCl_2$, $NiCl_2$, and $K_2Cr_2O_7$ mixture solution and the concentration of each heavy metal was 50 mg/100 mL; (c) Spray the contaminated solution on sand at the ratio of 1 mL: 10 g and mix them uniformly; (d) Take the sand to vacuum drying at 40 °C for 24 h; (e) Then, the sand was saturated with 1.5 pore volume of deionized water and incubated at 40 °C for 48 h; (f) After that, the sand was vacuum-dried at 40 °C and the dried sand was used as the artificially contaminated sand. The artificially contaminated sand was filled into a cylindrical mold (50 mm × 100 mm) in layers and compacted to a relative density of 48 % (1.652 g/cm^3). The mold was designed with an open top, and a small hole with 10 mm in diameter was drilled at the bottom to facilitate drainage. Additionally, a 300-mesh nylon net was placed at the bottom of the mold to serve as a filtration layer. The pore volume of each artificially contaminated sand specimen was 74 mL.

Later on, the Tessier Sequential method was used to quantify the exchangeable fraction of Zn, Ni, and Cr(VI) in contaminated sand (Tessier et al., 1979). It is reported that the exchangeable fraction comprises the mobile form of heavy metals in soils and is easily released into the environment, which shows a strong correlation with toxicity (Akbarpour et al., 2021; Devi and Saroha, 2014). The results in Supplemental file S4-Table. 2 showed that the exchangeable fraction of Zn, Ni, and Cr(VI) measured by Tessier Sequential method was about 39.29–43.53 %, 42.73–47.25 %, and 46.66–49.16 % of the total amount of heavy metals in contaminated sand, respectively.

It should be pointed out that according to the risk control standard for soil contamination of agricultural land (GB15618–2018), the risk screening values for Zn, Ni, and Cr(VI) are 300, 190, and 200 mg/kg, respectively, when pH > 7.5. As mentioned in Introduction, the accumulated contaminated soil is subject to risks of heavy metal leaching and slope instability. The tailings reservoir and landfills are barely used as agricultural land for cultivation. In this study, the total amount of Zn, Ni, Cr(VI) in artificially contaminated sand was 50 mg/kg, respectively. The leaching concentrations of Zn, Ni, Cr(VI) of artificially contaminated sand in this study were about 2.45–2.72 mg/L, 2.67–2.95 mg/L, and 2.91–3.07 mg/L, respectively. Studies have reported that the leaching concentrations of Zn, Ni, and Cr(VI) of contaminated soil in landfills ranged from 0.671–56.11 mg/L, 0.007–3.10 mg/L, and 0.049–2.47 mg/L (Karnchanawong and Limpiteeprakan, 2009; Liu and Sang, 2010; Shi and Kan, 2009; Zhang et al., 2008; Zheng et al., 2022). Therefore, the

concentrations of Zn, Ni, and Cr(VI) in this study represent the typical levels of contaminated soils in landfills.

2.3. Immobilization of heavy metals in liquid batch tests

To better mimic mobile heavy metal environment in sand, the concentration of each heavy metal in the subsequent liquid batch test would be considered at 50 % of the total amount of heavy metals in sand. Specifically, the volume of EICP-treatment solution added each time was one pore volume of sand specimen, that is 74 mL. Assuming that the exchangeable heavy metals in contaminated sand (considered as 50 % of the total amount of heavy metals) were completely dissolved in one pore volume solution, the concentration of each heavy metal in solution was 109 mg/L. Therefore, the concentration of each heavy metal is 109 mg/L in liquid batch tests.

The contaminated soil from landfills typically contains multiple heavy metal ions, including both anions and cations. In particular, soil contaminated with Cr(VI) is often accompanied by other heavy metal cations, such as Zn, Ni, Cu, Pb, and Cd (Kasassi et al., 2008; Kumpiene et al., 2008). In soil, the exchangeable Zn, Ni, and Cr(VI) coexist, with their respective forms being Zn^{2+}, Ni^{2+}, and $Cr_2O_7^{2-}/CrO_4^{2-}$. In order to investigate the effect of EICP-treatment on the urease activity and immobilization of heavy metals (i.e. Zn, Ni, and Cr(VI)), four groups of liquid batch tests were conducted. The detailed arrangements are listed in Supplemental file S5-Table. 3. Three for EICP-treatment with different individual heavy metal (denoted as Group-$Zn_{0/0.25/0.5}$, Group-$Ni_{0/0.25/0.5}$, Group-$Cr_{0/0.25/0.5}$) to investigate the immobilization mechanism of individual heavy metal. One for EICP-treatment with multiple heavy metals (denoted as Group-$multiple_{0/0.25/0.5}$) to investigate the immobilization mechanism of multiple heavy metals. To evaluate the impact of calcium carbonate on the heavy metal immobilization, the concentrations of urea and calcium chloride in each group were 0.75 mol/L and 0/0.25/0.5 mol/L, respectively. 0/0.25/0.5 refers to the Ca^{2+} concentration, e.g. Group-$Ni_{0.25}$ means the Ni^{2+} contaminated solution treated by EICP method with 0.25 mol/L Ca^{2+}. 0.75 mol/L of urea was used in this study, which is based on the theoretical requirement of an excess of 0.5 mol/L urea to achieve maximum precipitation efficiency of calcium carbonates since the highest Ca^{2+} concentration added was 0.5 mol/L, as adopted in many references (Ahenkorah et al., 2020; Almajed et al., 2018). Additionally, previous studies have also shown that urea concentrations below 1 mol/L can maintain a high level of urease activity (Ahenkorah et al., 2020; Xie et al., 2023). Hence, a concentration of 0.75 mol/L urea was selected.

Before the bio-immobilization process, the individual and multiple heavy metals contaminated solutions were prepared by dissolving the relevant salts (i.e. $ZnCl_2$, $NiCl_2$, and $K_2Cr_2O_7$) in deionized water. In the liquid batch tests, urea and calcium chloride ($CaCl_2$) were added into sword bean urease solution, referred to as the EICP-treatment solution. Then, heavy metal contaminated solutions were mixed with the EICP-treatment solution with equal volume. After mixing the EICP-treatment solution with aqueous heavy metal solution, the initial concentration of each heavy metal, sword bean urease, urea, and calcium chloride were 109 mg/L, 20 g/L, 0.75 mol/L, and 0/0.25/0.5 mol/L, respectively. All the chemical used were of analytical reagent grade. Each test group was set with three replicates at 25 °C. The urea hydrolysis completion efficiency (the measured ammonium concentration divided by the theoretical ammonium concentration obtained by complete hydrolysis of urea), pH, Ca^{2+} immobilization percentage, and heavy metal immobilization percentage variation of the samples were measured continuously until the results remain stable and unchanged. The residual concentration of Ca^{2+} and heavy metals in solution were measured using the ICP-MS (PerkinElmer NexION 300×, USA). The immobilization percentage of both Ca^{2+} and heavy metals was calculated by ratio of the concentration of immobilized metal ions to the total concentration of added metal ions. After the reaction was complete, the samples were filtered using a filter paper to separate the precipitates from the solutions.

2.4. Immobilization of heavy metals and unconfined compressive strength (UCS) test in contaminated soil

To investigate the effect of the EICP-treatment on immobilization of Zn^{2+}, Ni^{2+}, and Cr(VI) in contaminated sand, three groups of sand specimens were prepared: (a) contaminated sand specimens treated with sword bean urease and 0.75 mol/L urea solution; (b) contaminated sand specimens treated with sword bean urease and 0.75 mol/L urea +0.25 mol/L calcium chloride solution; (c) contaminated sand specimens treated with sword bean urease and 0.75 mol/L urea +0.50 mol/L calcium chloride solution. Each group underwent treatment cycles ranging from 1 to 4, with each specimen consisted of four parallel columns. The EICP-treatment solutions were percolated into sand specimens from top to bottom, and each cycle included one percolation of the treatment solution (Almajed et al., 2018; Liu et al., 2023a).The whole protocol of the sand treatment experiments was summarized in Supplemental file S6-Table. 4.

Approximately 74 mL of the EICP-treatment solution, equivalent to the pore volume of the untreated sand specimen, was percolated from top to bottom of the sand specimen (see Section 2.2). All percolations were conducted under free drainage, with a 48-h interval between consecutive percolation events. During each percolation, the outflow was collected and concentration of heavy metal ions and Ca^{2+} were determined by ICP-MS. After that, the sand specimens were cured at 25 °C for 48 h. Subsequently, the sand specimens were oven-dried at 60 °C (Qi et al., 2022) before undergoing unconfined compressive strength (UCS) testing. The UCS test was used to evaluate the strength of the bio-cemented soil. The testing procedures strictly followed ASTM standards (ASTM, 2010). After UCS test, the exchangeable fraction of heavy metal in treated sand specimens was measured using Tessier Sequential method. The immobilization percentage was calculated by the concentration of immobilized metal ions after EICP-treatment divided by the concentration of exchangeable heavy metals before treatment. The $CaCO_3$ content of treated sand specimen was measured by acid dissolving method (Cui et al., 2024; Xiao et al., 2019): (a) The sand were carefully rinsed with deionized water three times to remove soluble salts; (b) Then, they were soaked into 1 mol/L hydrochloric acid for 24 h to fully dissolve calcium carbonate; (c) The concentration of Ca^{2+} in acid solution was measured by ICP-MS, and total mass of $CaCO_3$ was determined by the multiplication of Ca^{2+} concentration, volume of acid dissolving solution, and molecular weight of $CaCO_3$. (d) The $CaCO_3$ content (%) can be calculated by total mass of $CaCO_3$ divided by total mass of sand.

2.5. XRD, FTIR and SEM-EDS analysis

The microscopic characteristics of the precipitates in solutions and EICP-treated sands were explored by X-ray diffraction (XRD, Bruker D8 Advance, Germany), FTIR (PerkinElmer Spectrum Two FT-IR Spectrometer, USA), and scanning electron microscopy (SEM, FEI Quanta 650 FEG SEM, USA) with energy dispersive X-ray (EDS) analysis.

3. Results and discussion

3.1. Results in liquid batch tests

According to Eqs. (1)–(4) in Introduction, 1 mol of urea can produce 2 mol of NH_3 and 1 mol of CO_2. Then, 1 mol of NH_3 reacts with water to form ammonium ions (NH_4^+) and hydroxide ions (OH^-), which may increase the pH of the solution. The CO_2 dissolves in water and dissociates into CO_3^{2-} in alkaline solution eventually. Further, the CO_3^{2-} combine with Ca^{2+} to form $CaCO_3$ precipitation. In the entire solution system, the hydrolysis of urea causes an increase in pH, while the generation of $CaCO_3$ causes a decrease in pH. The changes in the solution pH

are the result of the combined effects of these two reactions. When the EICP processes are complete, the pH of the solution increases in this study. Assuming complete hydrolysis of 0.75 mol/L urea and not considering the escape of gas, it will theoretically produce 1.5 mol/L NH_4^+ and 0.75 mol/L of CO_3^{2-}. Simultaneously, 0.75 mol/L of CO_3^{2-} will be generated. In alkaline solution, these 0.75 mol/L of CO_3^{2-} will react with 0.25 mol/L or 0.5 mol/L of Ca^{2+}, theoretically generating 0.25 mol/L or 0.5 mol/L of $CaCO_3$, respectively.

Studies have found that environmental factors such as temperature and pH may change the urease activity, thereby affecting EICP process. The optimal temperature and pH for urease activity ranges from 40 °C to 60 °C and 9 to 11, respectively (Ahenkorah et al., 2021; Krajewska, 2016; Xie et al., 2023). In addition, the heavy metals such as Fe^{3+}, Mn^{2+}, Cu^{2+}, and Pb^{2+} often exist in contaminated water in practice (Han et al., 2016, 2015). These heavy metal ions can also affect urease activity to different degrees. Wang et al. (2022) have explored the effectiveness of EICP in remediating Cu^{2+} and Pb^{2+} contaminated solution. They found that as the concentration of Pb^{2+} increased, the final hydrolysis completion efficiency of urea gradually decreased; meanwhile, urease lost its activity quickly due to the toxicity of Cu^{2+}. The effects of other heavy metal ions, such as Fe^{3+} and Mn^{2+}, on the EICP process, have not yet been investigated. However, considering that the toxicity of these heavy metals can reduce urease activity, it may further decrease the urea hydrolysis rate and the reaction completion time will be longer.

3.1.1. *pH, urea hydrolysis completion efficiency, and Ca^{2+} immobilization percentage*

Fig. 1(a)–(d) illustrates the variations in pH for Group-Zn, Group-Ni, Group-Cr, and Group-multiple after reacting for 3, 6, 9, 12, 24, 36, 48, 60, 72, 84 h. It can be seen that the initial values of pH for all groups were ranging from 4.2 to 6.9, which were acidic and within the common pH range of heavy metal contaminated water in practice (Chen et al., 1997; Jiménez-Rodríguez et al., 2009). In each group without Ca^{2+} added, the initial pH was 4.6–6.3. Then, the pH increased and stabilized at 9.2–9.4 after 6 h reaction. The increased pH was attributed to the produced OH^- during the urea hydrolysis process. For Group-$Zn_{0.25/0.5}$, Group-$Ni_{0.25/0.5}$, Group-$Cr_{0.25/0.5}$, and Group-$multiple_{0.25/0.5}$, the initial pH ranged from approximately 4.2 to 6.9. Then, the pH increased steadily and stabilized at 9.0–9.1 and 8.6–8.7 after 24 h reaction. In Group-$multiple_{0.25/0.5}$, there is a notable difference in the changes of pH. Specifically, this difference manifested as the delayed stabilization time, reaching around 48 to 60 h. Besides, the final pH in Group-$multiple_{0.25/0.5}$ was declined by 0.6–0.7 compared to Group-Zn/Ni/Cr(VI)$_{0.25/0.5}$. The reduction in pH was a result of decrease in urea hydrolysis completion efficiency.

Fig. 2(a)–(d) shows the variations in urea hydrolysis completion efficiency for Group-Zn, Group-Ni, Group-Cr, and Group-multiple after reacting for 3, 6, 9, 12, 24, 36, 48, 60, 72, 84 h. In Group-Zn_0, Group-Ni_0, Group-Cr_0, and Group-$multiple_0$, the initial urea hydrolysis rate (defined as the slope of the urea hydrolysis completion efficiency curve) was significantly high, with around 85–90 % of urea being hydrolyzed within first three hours. After that, urea hydrolysis rate became much lower within 6 to 9 h. The final urea hydrolysis completion efficiency for Group-Zn_0, Group-Ni_0, Group-Cr_0, Group-$multiple_0$ was 99.9 %, 99.9 %, 99.9 %, and 93.6 % respectively. This indicates that, multiple heavy metals would influence sword bean urease catalytic capacity without Ca^{2+} addition, leading to about 6.3 % reduction in urea hydrolysis completion efficiency. With the increase of Ca^{2+} concentration, there was a decrease in both initial urea hydrolysis rate and final completion efficiency in all groups. Notably, the most pronounced reduction was observed in Group-$multiple_{0.25/0.5}$, wherein urea could only be hydrolyzed 86 % and 62 %, respectively. This may be caused by more toxicity of multiple heavy metals than individual heavy metal to urease extracts, and the Ca^{2+} intensified the influence.

Fig. 2 also presents the impact of Ca^{2+} addition on urease activity throughout the reaction process. The urease activity, also known as urea hydrolysis rate, can be calculated by the changes of urea hydrolysis completion efficiency with time. In the initial 3 h, higher Ca^{2+} in each group resulted in lower initial urea hydrolysis completion efficiency, which was consistent with the findings of Xie et al. (2023) and Whiffin

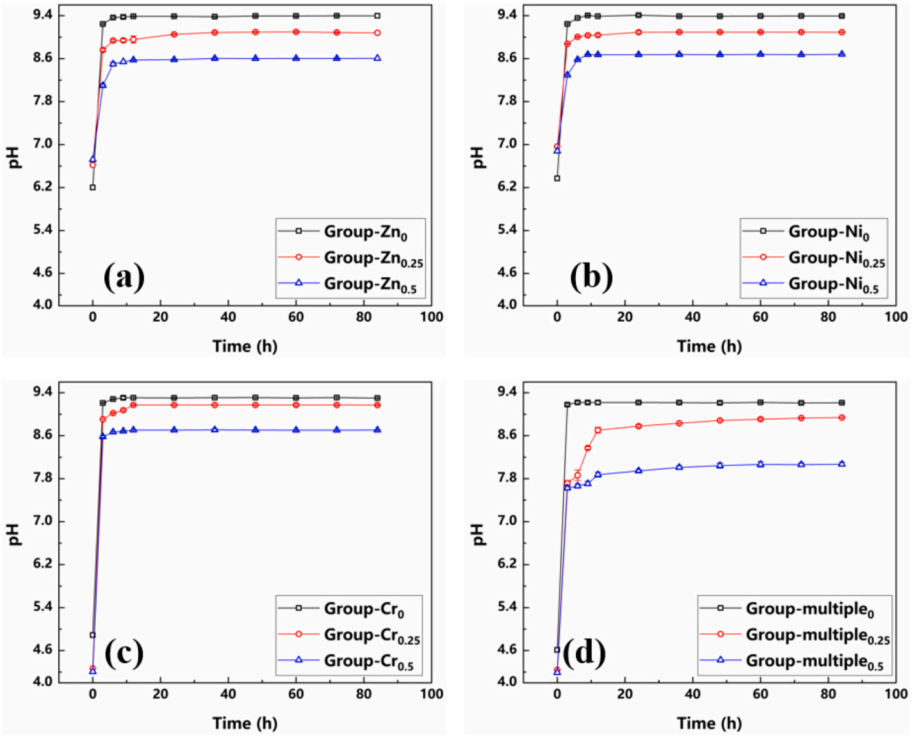

Fig. 1. Variations in pH with time in solutions (a) Group-$Zn_{0/0.25/0.5}$; (b) Group-$Ni_{0/0.25/0.5}$; (c) Group-$Cr_{0/0.25/0.5}$; (d) Group-$multiple_{0/0.25/0.5}$. (Data are presented in mean ± standard error of mean, $n = 3$.)

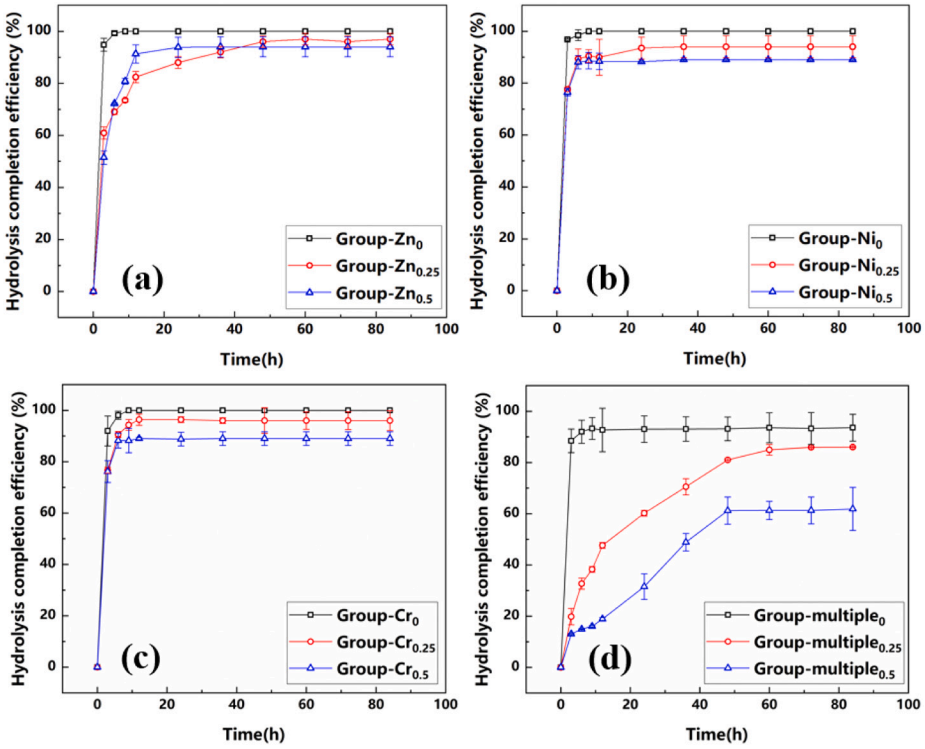

Fig. 2. Variations in urea hydrolysis completion efficiency with time in solutions: (a) Group-$Zn_{0/0.25/0.5}$; (b) Group-$Ni_{0/0.25/0.5}$; (c) Group-$Cr_{0/0.25/0.5}$; (d) Group-$multiple_{0/0.25/0.5}$.
(Data are presented in mean ± standard error of mean, n = 3.)

(2004). This can be attributed to the higher concentration of Ca^{2+} in the intensified complexation and salting-out effects with urease protein, thereby inhibiting urease activity (Dinesh et al., 1995; Hidri et al., 2022; Knape et al., 2015; Liu et al., 2023b; Maeda et al., 1990). As the urea continuously hydrolyzed, the urea hydrolysis completion efficiency in the Group-$Ni_{0.5}$, Group-$Cr_{0.5}$, and Group-$multiple_{0.5}$ remained consistently lower than in the Group-$Ni_{0.25}$, Group-$Cr_{0.25}$, and Group-$multiple_{0.25}$, respectively. This may result from the change of three-dimensional structure of urease proteins by Ca^{2+}, which consequently affects the activity (Lee et al., 2017). However, in the Group-$Zn_{0.25/0.5}$, a different phenomenon was observed: the urease activity in the Group-$Zn_{0.5}$ was initially lower than that in the Group-$Zn_{0.25}$ but later surpassed it during some time, and the final urea hydrolysis completion efficiency of Group-$Zn_{0.5}$ was lower that of the Group-$Zn_{0.25}$. The underlying mechanism for this observation could be explained by the influence of Ca^{2+}. In the initial stage of the reaction (0−3h), the inhibition of urease activity due to the complexation and salting-out effect for Group-$Zn_{0.5}$ was more obvious than that for Group-$Zn_{0.25}$. As a result, the initial urease activity of Group-$Zn_{0.5}$ was lower than that of the Group-$Zn_{0.25}$, leading to a lower urea hydrolysis completion efficiency in the first 3 h. However, the complexation and salting-out effect was unstable. As urea hydrolyzed, the produced CO_3^{2-} combined with Ca^{2+} to form calcium carbonate precipitates, potentially causing decomplexation between Ca^{2+} and urease protein (Deak et al., 2006; Horne, 1998; Zhang et al., 2017b). During this stage (3–12 h), the Ca^{2+} immobilization percentage of Group-$Zn_{0.5}$ (78.2 % to 98.8 %) was always lower than that of Group-$Zn_{0.25}$ (98.9–99.6 %), indicating more Ca^{2+} in solution of Group-$Zn_{0.5}$. The small amount of Ca^{2+} in solution of Group-$Zn_{0.5}$ provided a protective effect for urease in Zn^{2+} solution (Wang et al., 2023c; Xie et al., 2024). In contrast, the Ca^{2+} in the Group-$Zn_{0.25}$ were almost completely immobilized, which could not protect urease activity. Consequently, urease activity in the Group-$Zn_{0.5}$ was higher than that in the Group-$Zn_{0.25}$ at this stage (3–12 h), leading to a higher urea hydrolysis completion efficiency and higher concentration of NH_4^+. During 12 to 24 h, the urease activity in the Group-$Zn_{0.5}$ group further decreased due to the inhibitory effect of more NH_4^+ on urease (Almajed et al., 2018; Hu et al., 2021b; Li et al., 2022; Meng et al., 2021). As a result, urea hydrolysis in Group-$Zn_{0.5}$ ceased at around 24 h. In contrast, the urease activity in the Group-$Zn_{0.25}$ had less inhibition from NH_4^+, allowing the reaction to proceed slowly and steadily until it stabilized around 48 h. Ultimately, the hydrolysis completion efficiency in the Group-$Zn_{0.25}$ slightly surpassed that of the Group-$Zn_{0.5}$.

Fig. 3 describes the changes in the Ca^{2+} immobilization percentage in solutions of Group-Zn, Group-Ni, Group-Cr, and Group-multiple. It can be found that the variation in Ca^{2+} immobilization process in Group-Zn, Group-Ni, Group-Cr, and Group-$multiple_{0.25}$ can be divided into three stage, namely rapid reaction stage, slower reaction stage, and stable stage. Rapid reaction stage was 0–3 h in Group-Zn, -Ni, and -Cr (VI) while 0–6 h in Group-multiple due to the high urease activity at the beginning. Slower reaction stage was 3–12 h in Group-Zn, -Ni, and -Cr while 6–48 h in Group-multiple owing to the gradual decrease in urease activity. After 12 and 48 h, the stable stage of Ca^{2+} immobilization percentage can be found in Group-individual and Group-multiple, respectively. The changes in Ca^{2+} concentration was in agreement Yuan et al. (2020), who investigated the changes in residual Ca^{2+} concentration with respect to reaction time in EICP process.

The findings presented in Fig. 3 also revealed that Ca^{2+} immobilization percentage remained unaffected by the coexisting of individual Zn, Ni or Cr (VI), and Ca^{2+} was almost completely removed. In Group-$multiple_{0.25}$, Ca^{2+} was 99.9 % immobilized while Ca^{2+} was 93 % immobilized in Group-$multiple_{0.5}$. The immobilization of Ca^{2+} was mainly dependent on forming calcium carbonate precipitation with the hydrolyzed CO_3^{2-} from urea (Liu et al., 2023a). Therefore, the changes in the Ca^{2+} immobilization percentage were related to the urea hydrolysis completion efficiency. In Group-$Zn_{0.25/0.5}$, -$Ni_{0.25/0.5}$, and -$Cr_{0.25/0.5}$, urea hydrolysis completion efficiency was high, with enough CO_3^{2-} produced within first three hours, contributing to over 99 % formation of $CaCO_3$ since the concentration of urea was 0.75 mol/L. Despite the

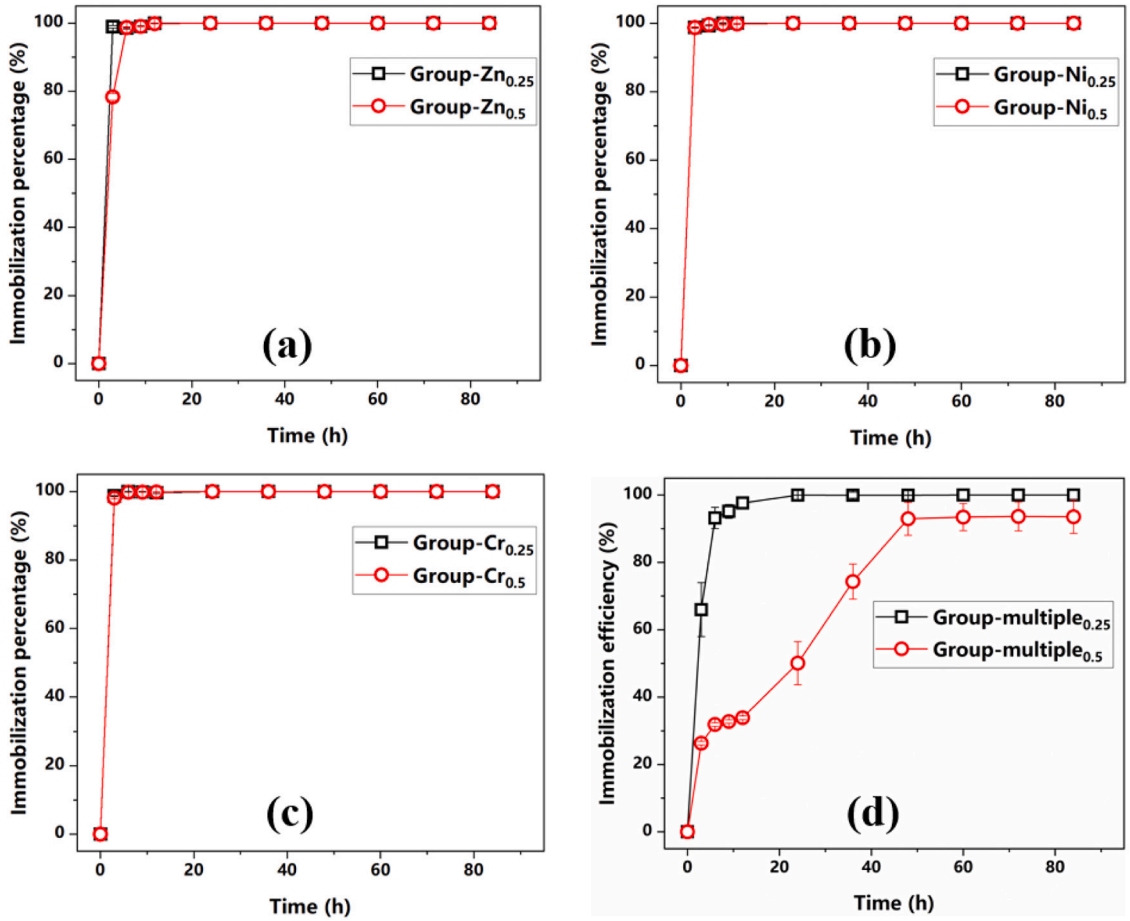

Fig. 3. Variations in Ca^{2+} immobilization percentage with time in solutions (a) Group-$Zn_{0.25/0.5}$; (b) Group-$Ni_{0.25/0.5}$; (c) Group-$Cr_{0.25/0.5}$; (d) Group-$multiple_{0.25/0.5}$. (Data are presented in mean ± standard error of mean, n = 3.)

urea hydrolysis completion efficiency in Group-$multiple_{0.25}$ being only 86 %, it was sufficient to generate CO_3^{2-} and form $CaCO_3$. The final Ca^{2+} immobilization percentage of Group-$multiple_{0.25}$ was 99.9 %. In Group-$multiple_{0.5}$, nevertheless, the final Ca^{2+} immobilization percentage was 7 % lower compared to other groups, possibly attributed to lower urea hydrolysis completion efficiency.

3.1.2. *Heavy metal immobilization percentage in solution*

In order to evaluate the immobilization of individual and multiple heavy metals in solutions of EICP method, the heavy metal immobilization percentage in each group was measured. Fig. 4 represents the variation in heavy metal immobilization percentage with time for both individual and multiple groups without Ca^{2+} added. Generally, the heavy metal immobilization percentage increased rapidly during first three hours. During 3 to 9 h, a slow increase of the heavy metal immobilization percentage was observed. After 9 h of reaction, a stable state of heavy metal immobilization percentage was achieved. Comparing the heavy metal immobilization percentage of Group-Zn_0, Group-Ni_0, and Group-Cr_0, EICP treatment was most effective in immobilizing Zn^{2+}(49.9 %), followed by Ni^{2+}(18.3 %) and Cr(VI)(10.5 %). Similar tendency was also observed in Group-$multiple_0$ and the immobilization percentage of each heavy metal in Group-$multiple_0$ was lower than that in Group-Zn_0, Group-Ni_0, and Group-Cr_0, respectively. Specifically, the final immobilization percentage of Zn, Ni, and Cr for Group-$multiple_0$ were 39.9 %, 13.8 %, and 7.9 %, respectively, which is 10 %, 4.5 %, and 2.6 % lower than that for Group-Zn_0, Group-Ni_0, and Group-Cr_0.

Heavy metal in groups without Ca^{2+} addition was immobilized mainly through biomineralization: heavy metal ions combine with CO_3^{2-} or OH^- to form heavy metal carbonate and hydroxide. In both individual and multiple groups, the immobilization percentage followed the order $Zn^{2+} > Ni^{2+} > Cr(VI)$, a trend attributed to solubility product (K_{sp}). The K_{sp} values of $ZnCO_3$ and $Zn(OH)_2$ are markedly lower than those of $NiCO_3$ and $Ni(OH)_2$, making Zn^{2+} much easier to form carbonate and hydroxide. It is difficult for Cr(VI) to form carbonate and hydroxide precipitates due to its unique properties, which led to the lowest immobilization percentage. Furthermore, the immobilization percentage of each heavy metal in Group-multiple was inferior to that in individual groups, possibly owing to the diminished urease activity in Group-multiple, consequently influencing urea hydrolysis and pH, thereby limiting heavy metal immobilization.

Research also reported that the crude sword bean urease solution contains rich organic molecules, such as amino acids, proteins, and polysaccharides (Khodadadi Tirkolaei et al., 2020; Liu et al., 2023a). In addition to the aforementioned mechanisms, heavy metal might also be immobilized by adsorption or complexation of organic molecules (amino acid, protein, polypeptide, and polysaccharide) in sword bean urease, (Blundell and Jenkins, 1977; Da Silva and Williams, 2001; Yang et al., 2019). Studies have demonstrated that the functional groups of organic molecules such as carbonyl, carboxyl, amino, and hydroxyl could be involved in the complexation process with heavy metals. The difference in immobilization percentage among Zn, Ni, and Cr(VI) might be also caused by various interactions between organic molecules and heavy metals. Liu et al. (2013) found the adsorption capacity of soy protein to heavy metal ions in solution was Zn > Ni > Cr. Given the structural resemblances between sword bean protein and soybean protein, it is rational to assume that in this study, the metal-binding capabilities of proteins in sword bean urease may present similar trend.

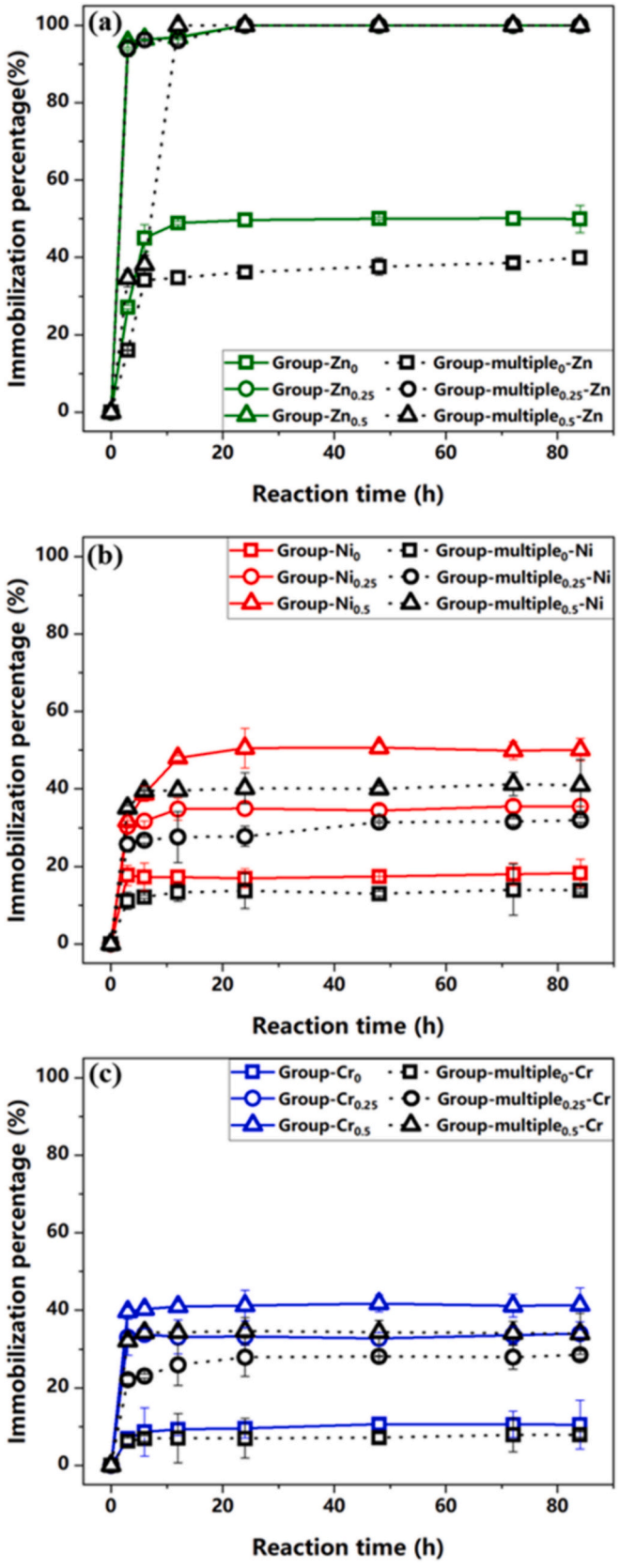

Fig. 4. Variations in heavy metal immobilization percentage with time in solutions: (a) Group-$Zn_{0/0.25/0.5}$ + Group-$multiple_{0/0.25/0.5}$-Zn; (b) Group-$Ni_{0/0.25/0.5}$ + Group-$multiple_{0/0.25/0.5}$-Ni; (c) Group-$Cr_{0/0.25/0.5}$ + Group-$multiple_{0/0.25/0.5}$-Cr.

Fig. 4 also shows the change in heavy metal immobilization percentage with the addition of Ca^{2+}. It is evident that heavy metal immobilization percentage increased with higher concentration of introduced Ca^{2+}. The highest heavy metal immobilization percentage was achieved when adding 0.5 mol/L Ca^{2+}, followed by the groups with 0.25 mol/L Ca^{2+}, and the groups without Ca^{2+} showed the lowest immobilization percentage, indicating that Ca^{2+} plays a role in heavy metals immobilization. In Group-Zn, -Ni, and -Cr, the EICP method with the addition of 0.25/0.5 mol/L Ca^{2+} was most effective in immobilizing Zn^{2+}, with final immobilization percentage of up to 99.9 %, experiencing an increase of 50 % compared to Group-Zn_0. Next was Ni^{2+}, with an immobilization percentage of approximately 35.48 %/50.14 %, increased by 17.18/31.84 % compared to Group-Ni_0. Cr(VI) had the lowest immobilization percentage at only about 34.0 %/41.36 % and was increased by 23.5 %/30.86 %, compared to Group-Cr_0. In Group-$multiple_{0.25/0.5}$, comparable trend could also be observed, and the immobilization percentage of each heavy metal in Group-$multiple_{0.25/0.5}$ was inferior to individual groups. The immobilization percentage of Zn^{2+} in Group-$multiple_{0.25/0.5}$ was close to that in Group-$Zn_{0.25/0.5}$, whereas immobilization percentage of Ni^{2+} and Cr(VI) reduced by 3.51–9.17 % and 5.49–7.38 %, respectively.

The groups with the addition of Ca^{2+} contributed to an increase in heavy metal immobilization compared to those without Ca^{2+}, indicating Ca^{2+} might have an influence on heavy metal immobilization. $CaCO_3$ has been widely confirmed as a metal adsorbent by physical adsorption or coprecipitation (Achal et al., 2012; Godelitsas et al., 2003; Sheng et al., 2023). Therefore, $CaCO_3$ adsorption may be considered as one of the immobilization mechanisms in EICP. Zn^{2+} may be effectively removed due to the remarkable adsorption capacity of $CaCO_3$ (Ahmad et al., 2012). Similarly, the Ni^{2+} can also be partially immobilized by adsorption/coprecipitation with $CaCO_3$ (Lakshtanov and Stipp, 2007; Vakili et al., 2021). The adsorption capacity of Cr(VI) onto $CaCO_3$ was investigated by Vu et al. (2019) and Nkutha et al. (2021). They reported that the adsorption capacity of Cr(VI) onto $CaCO_3$ decreases as pH increases, achieving an adsorptive capacity of approximately 20 mg/g at a solution pH of 8–9. The adsorptive mechanisms can be attributed to surface complexation caused by the high reactivity of the adsorbents functional group (-C=O) in the carbonate towards Cr(VI), hydrogen bonding interactions between (-C=O) and $HCrO_4^-$, and electrostatic attraction. Hence, $CaCO_3$ have different adsorption/complexation effect on various heavy metals.

3.1.3. *Identification of heavy metal-containing precipitates of liquid batch test*

Fig. 5(a) presents the XRD patterns of Zn-, Ni-, Cr-containing precipitates in liquid batch test with the addition of 0.5 mol/L Ca^{2+}. In all groups, calcite is the major mineral due to the much higher concentration of added Ca^{2+} compared to heavy metals. Besides, the 25.1°, 27.2°, and 71.5° are the typical peak values of $ZnCO_3$, $Zn(OH)_2$, and $NiCO_3$, respectively (Li et al., 2017; Liang et al., 2022; Rosado-Mendoza et al., 2018). The presence of trace $ZnCO_3$ and $NiCO_3$ crystals in Group-Zn/Ni confirmed that the immobilization mechanism of Zn^{2+} and Ni^{2+} were partially dependent on the biomineralization induced by sword bean urease. Additionally, the XRD results of Group-Zn validated the existence of $Zn(OH)_2$, implying that Zn immobilization also relied on the pH increase during EICP process. On the contrary, in Group-Cr, neither heavy metal carbonate precipitates nor metallic oxide were found. The XRD results of groups containing Cr(VI) revealed that the immobilization mechanism of Cr(VI) was quite different from Zn and Ni, which may be caused by special properties of $Cr_2O_7^{2-}$. In alkaline solution, the $Cr_2O_7^{2-}$ will transform into CrO_4^{2-} (Smith et al., 1989), but the $CaCrO_4$ precipitation was hardly observed for its lower ion activity product (IAP). Hence, in Group-Cr_0, Cr(VI) might be absorbed and complexation by organic molecules in crude urease extracts; In Group-$Cr_{0.25/0.5}$, the Cr (VI) could be immobilized through adsorption or complexation by both $CaCO_3$ and organic molecules.

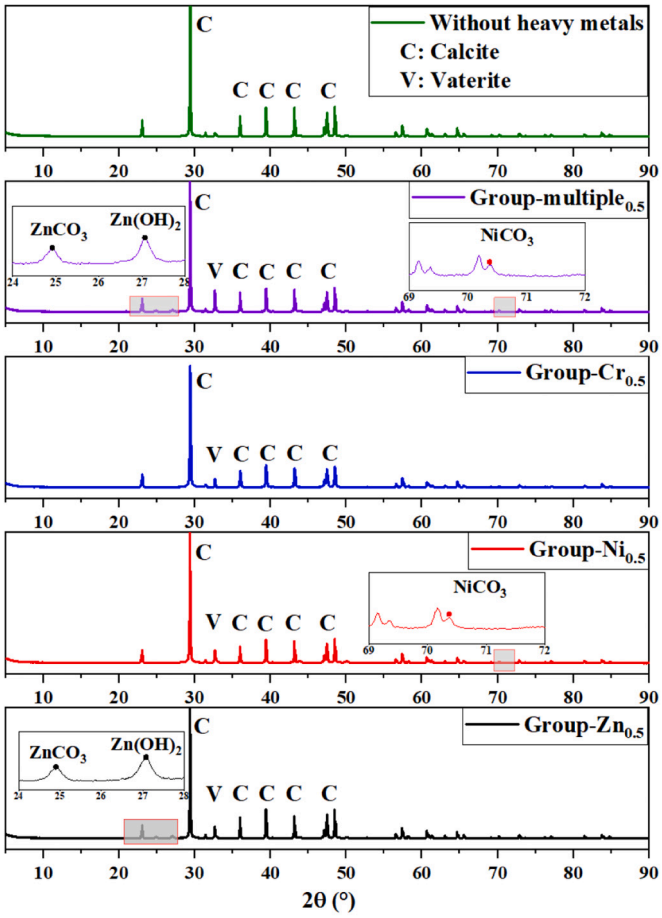

(a)

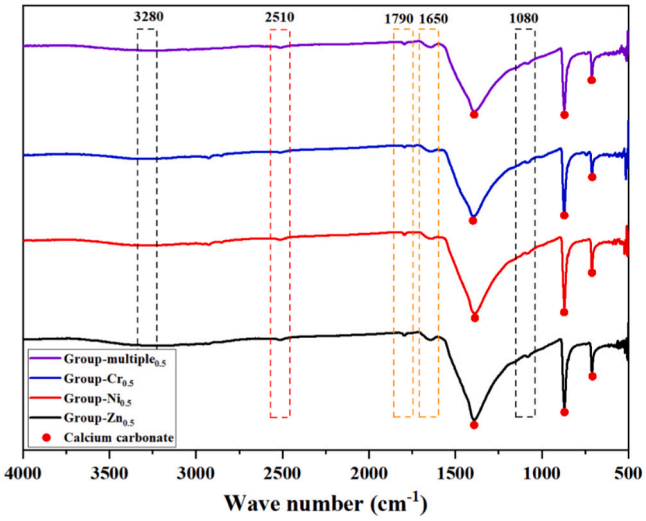

(b)

Fig. 5. Microscale analysis of precipitates in solutions: (a) XRD results; (b) FTIR results; (c) SEM-EDS results.

Apart from heavy metal precipitation, the crystalline phase of $CaCO_3$ also deserves our attention. Fig. 5(a) also shows the comparison of the XRD results of $CaCO_3$ with or without the addition of heavy metals. In all groups, the calcite was the dominant crystalline phase. In groups without heavy metals addition, the calcite dominated and vaterite was scarcely detected; while in groups with heavy metals, vaterite peaks were easily observed. This may be attributed to the presence of heavy metal ions, which can significantly impact the nucleation and growth of calcium carbonate crystals, ultimately influencing the crystallization phase. It is reported that Zn^{2+} has the ability to inhibit the transformation from vaterite to calcite (Freij et al., 2005; Tang et al., 2010). Sánchez-Pastor et al. (2011) found that the addition of Cr(VI) inhibited

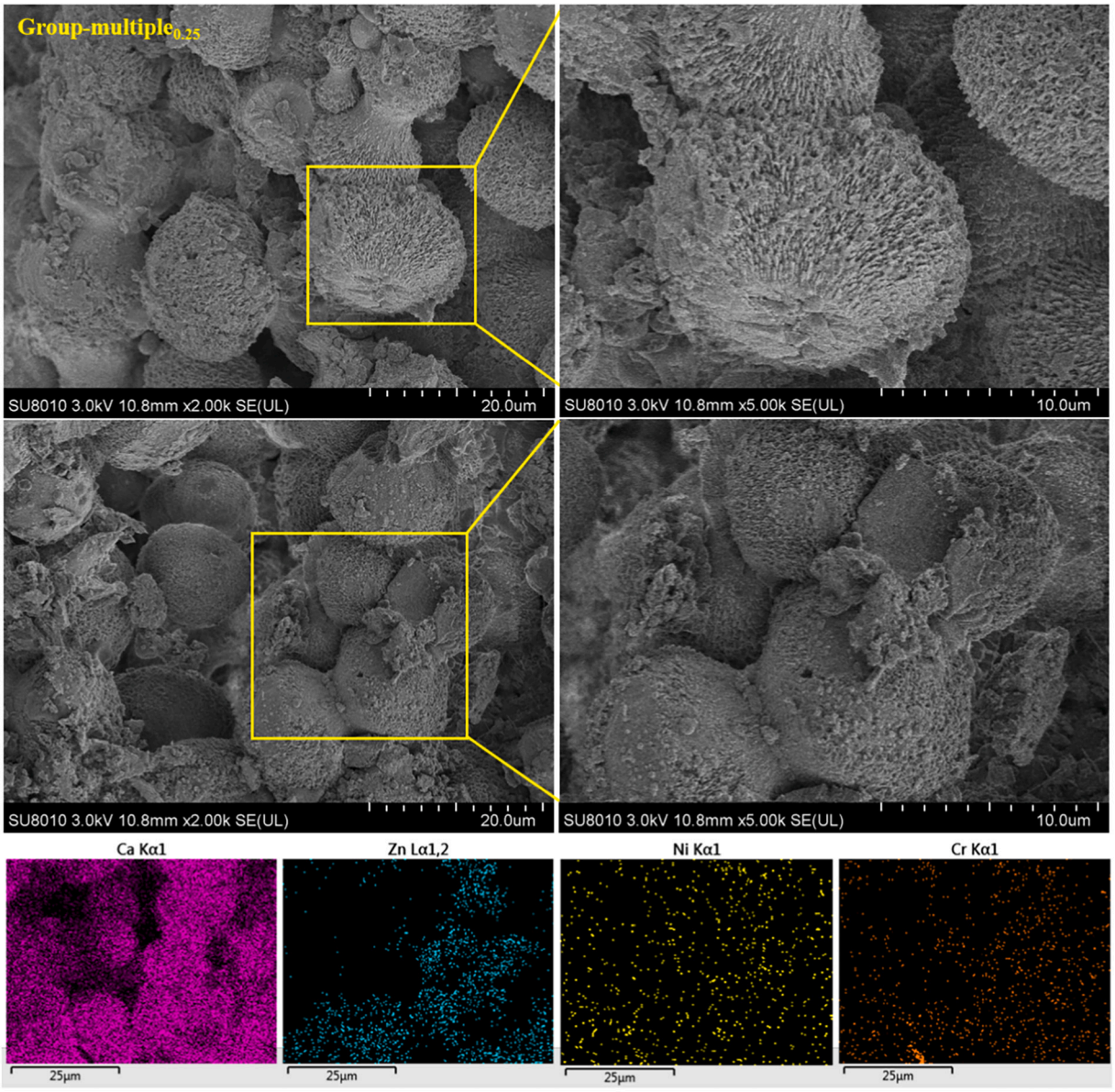

(c)

Fig. 5. (*continued*).

the nucleation and growth of calcite and promoted the formation of the metastable aragonite and vaterite. Matsumoto et al. (2010) and Wada et al. (1995) investigated the effect of type and concentration of additives on the polymorph and morphology of $CaCO_3$, and found that in the presence of heavy metal ions, such as Ni^{2+} and Zn^{2+} as trace impurities, the metastable aragonite or vaterite tended to form. In comparison to calcite, vaterite is a less stable polymorph form with worse crystallinity. Research has previously reported that $CaCO_3$ crystalline phase determines adsorption ability towards heavy metal ions (Wang et al., 2020a; Zhang et al., 2022). Consequently, it is speculated that heavy metals may influence the crystalline phase of $CaCO_3$ during EICP process, and the different crystal phases, in turn, might play distinct roles in heavy metal immobilize.

Fig. 5(b) shows the FTIR spectra of Zn-, Ni-, Cr-containing precipitates of liquid batch test with the addition of 0.5 mol/L Ca^{2+}. The bands with strongest peak intensities at the 1389, 870, and 710 cm^{-1} referred to $CaCO_3$. Small bands around 3280 and 1080 cm^{-1} could be attributed to -OH stretch vibration of polysaccharides while bands in the range of 1600–1800 cm^{-1} were related to C═O stretch vibration of the peptide linkage (amide I) (Hu et al., 2011; Hua and Li, 2014; Li et al., 2019). The weak band at 2510 cm^{-1} might be due to -SH in organic molecules of sword bean urease (Hua and Li, 2014). FTIR results validated the existence of carboxyl, hydroxyl, and sulfhydryl in precipitates, providing reliable evidence for heavy metal immobilization by complexation or adsorption with organic molecules in crude urease extracts.

SEM-EDS results of Group-multilple$_{0.25}$ precipitates in liquid batch tests are shown in Fig. 5(c). Precipitates in liquid batch test are mainly composed of Ca, and the trace elements of Zn, Ni, and Cr (VI) could be detected, which were likely to be adsorbed by $CaCO_3$ precipitates or organic molecules in crude urease extracts. The high-magnification SEM-EDS images in Fig. 5(c) revealed that urease-induced calcium carbonate had a rough surface with numerous small pores. This porous structure suggests a larger specific surface area, providing more active adsorption sites for Zn, Ni, and Cr(VI) (Choi and Jang, 2008; Deze et al., 2012; Song et al., 2021).

3.2. Heavy metal immobilization in contaminated sand specimen

3.2.1. Heavy metal immobilization percentage in contaminated sand specimen

Fig. 6 depicts the immobilization percentage of Zn^{2+}, Ni^{2+}, and Cr (VI) in artificially contaminated sand specimens, which can be characterized by exchangeable fraction of heavy metals. The immobilization percentage increased with treatment cycles, after 4th treatment, the immobilization percentage of Zn^{2+}, Ni^{2+}, and Cr(VI) was 99.87–99.99 %, 83.43–86.38 % and 73.43–75.18 %, respectively. In accordance with the outcomes of the liquid batch test, the immobilization percentage of heavy metals in sand specimens increased with the addition of Ca^{2+}, indicating $CaCO_3$ adsorption or complexation was one of the mechanisms of heavy metal immobilization in contaminated sand. It could also be observed that bioremediation percentage following the order Zn^{2+} > Ni^{2+} > Cr(VI) after each treatment cycle, which was consistent with liquid batch tests. The findings indicate variations in the efficacy of the EICP method for immobilizing various heavy metals in contaminated soil.

Heavy metal in sand specimens without Ca^{2+} addition was immobilized mainly through biomineralization and adsorption/complexation by organic molecules in crude urease extracts. With Ca^{2+} added, the heavy metal immobilization in sand specimens also depended on adsorption/complexation by $CaCO_3$, as discussed in liquid batch tests. The immobilization percentage order of Zn^{2+} > Ni^{2+} > Cr(VI) is reasonable when considering K_{sp} and different adsorption/complexation capacity of organic molecules and $CaCO_3$, which was also mentioned in former section.

In contrast to the results obtained from the liquid batch tests, the immobilization percentage of Ni^{2+} and Cr(VI) in the contaminated soil increased a lot, while the adsorption capacity of $CaCO_3$ in enhancing heavy metal immobilization percentage appeared to be somewhat weakened. Specifically, without Ca^{2+} addition, the immobilization percentage of Zn^{2+}, Ni^{2+}, and Cr(VI) in sand specimens after 1st treatment cycle was 90.62 %, 74.35 %, and 65.24 %, respectively, increasing by 50.7 %, 60.5 %, and 57.3 %, compared to their immobilization percentage in liquid batch tests. After the addition of 0.25 mol/L and 0.5 mol/L Ca^{2+}, the immobilization percentage of Zn, Ni, and Cr(VI) in sand specimens increased by 8.5–9.3 %, 3.12–6.2 %, and 1.1–2.1 %, respectively, compared to specimens that without Ca^{2+} addition.

Several factors may explain the obtained phenomenon. In liquid batch tests, the heavy metals directly contacted with sword bean urease and poisoned urease protein as soon as they were mixed together. Instead, heavy metals are uniformly distributed on the surface of artificially contaminated sand, thereby mitigating the direct toxicity to urease protein. Essentially, sand particle might offer buffering effect for EICP method to meditate heavy metals, the similar pattern was presented in Kang et al. (2016). The $CaCO_3$ formed during EICP process could effectively fill soil pores, thus impeding migration and diffusion of heavy metal ions (Nam et al., 2016). Considering the uniform distribution of heavy metal ions, the presence of heavy metals in a certain region does not necessarily correspond to the generation of $CaCO_3$. Therefore, the adsorption capacity of $CaCO_3$ was significantly limited.

3.2.2. Identification of heavy metal-containing precipitates of EICP-treated sand

To further analyze the heavy metal immobilization, the EICP-treated sand specimens were examined by XRD spectroscopy and SEM-EDS analysis. The results were shown in Fig. 7(a)–(b).

Fig. 7(a) shows the XRD results of sand specimens after 4th treatment cycle. In groups without addition of Ca^{2+}, $Zn(OH)_2$, $Ni_2(CO_3)(OH)_2$, and $Zn_5(CO_3)_2(OH)_6$ were detected, with typical peak values are 27.2°, 55.4°, and 35.0°, respectively (Liu and Teng, 2018; Rosado-Mendoza et al., 2018; Zhang et al., 2020). These minerals validated the immobilization of heavy metals in soil was mainly dependent on the biomineralization process when Ca^{2+} weren't introduced. Meanwhile, the CrO

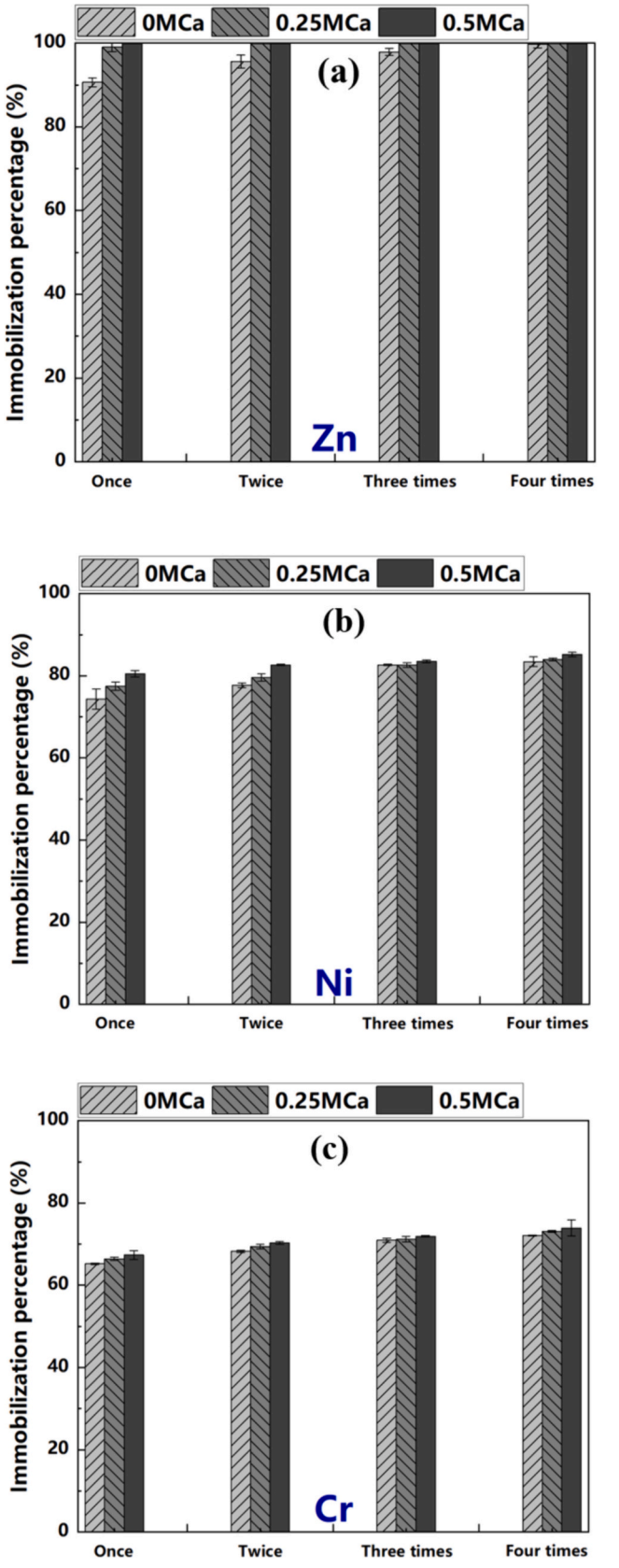

Fig. 6. Variations in heavy metal immobilization percentage with treatment cycles in sand specimens: (a) Zn^{2+}; (b) Ni^{2+}; (c) Cr(VI).

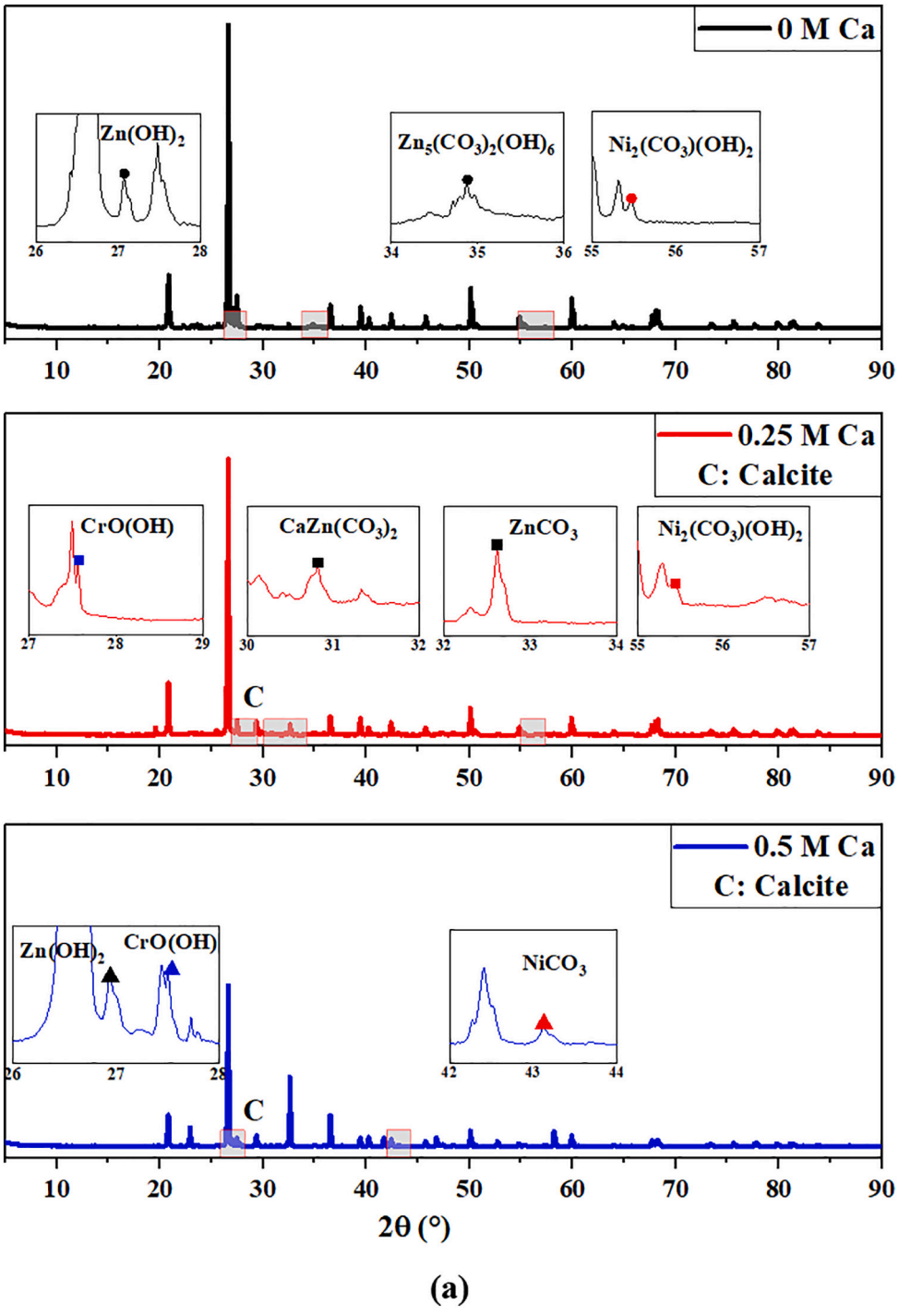

Fig. 7. Microscale analysis of EICP-treated sand: (a) XRD results; (b) SEM-EDS results.

(OH) was identified. This phenomenon may be due to the reductive functional groups within organic macromolecules, such as hydroxyl and carboxyl groups, facilitating the reduction of Cr(VI) to Cr(III). The subsequent formation of CrO(OH) occurred through the interaction of Cr (III) with OH^- in an alkaline environment. Similar results were found by Daneshvar et al. (2002), who demonstrated that hydroxyl or carboxyl groups in soybean cake could play a role in the reduction of Cr(III), consequently contributing to the removal of Cr(VI). It is worth mentioning that, the presence of $CaZn(CO_3)_2$ in the groups added Ca^{2+} suggested Zn^{2+} with an ion radius close to that of Ca^{2+} was incorporated into the $CaCO_3$ crystal by substituting the Ca^{2+} in the lattice or entering the interstices. From XRD spectroscopy results, it can also be observed that the $CaCO_3$ were predominately in the form of calcite, with vaterite scarcely detected. Former section has demonstrated the stability difference between calcite and vaterite, the predominance of calcite was advantageous for enhancing the strength of sand specimens. SEM-EDS results of treated-sand specimens are shown in Fig. 7(b). According to EDS analysis, trace elements of Zn, Ni, and Cr(VI) were detected, which were likely to be adsorbed by $CaCO_3$ or organic matter attached to sand particles.

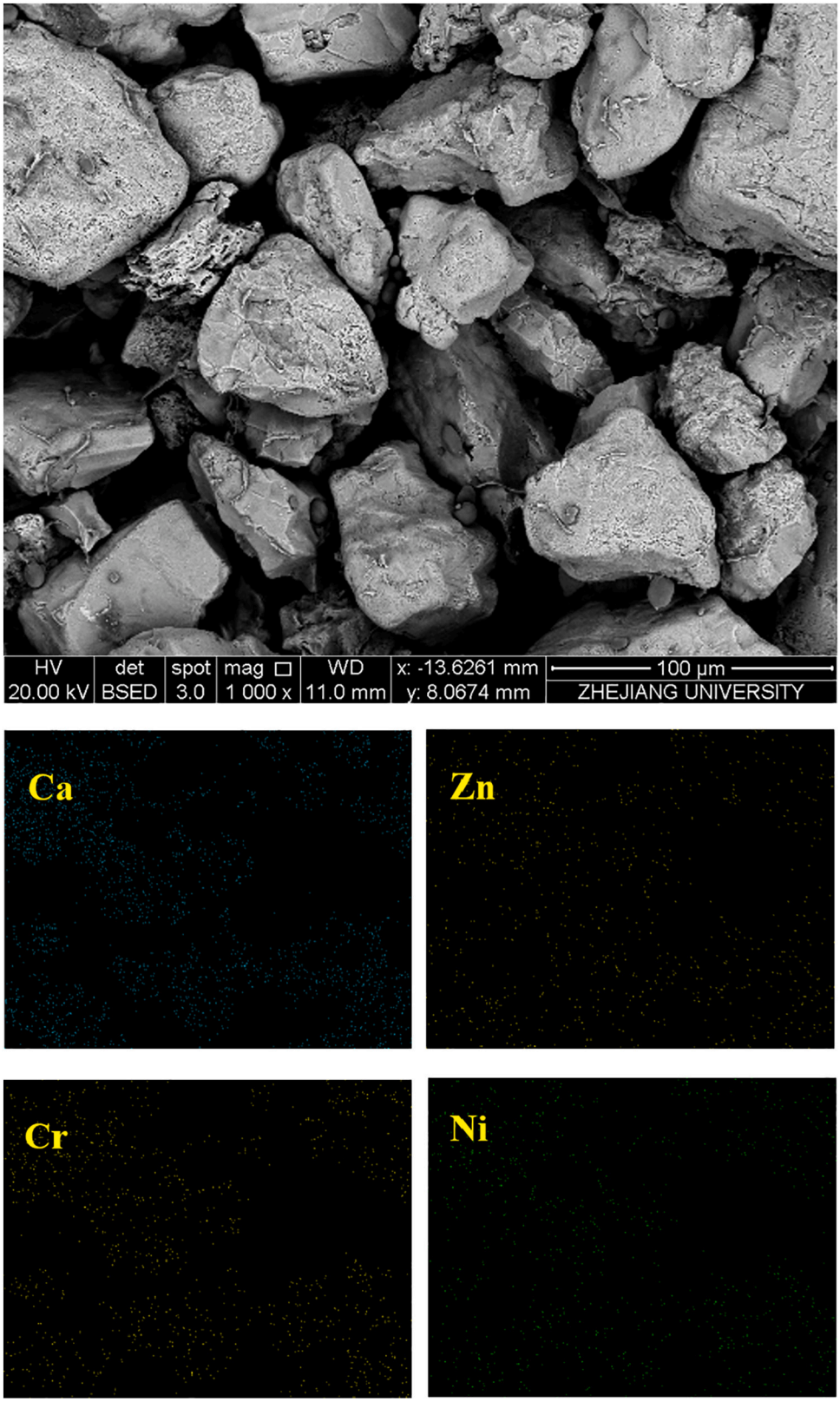

(b)

Fig. 7. (*continued*).

3.3. Strength improvement of EICP-treated contaminated sand specimen

3.3.1. UCS and calcium carbonate content

The Unconfined Compressive Strength (UCS) of sand is typically used to evaluate the shear strength of cemented sands, especially in geotechnical engineering (Meng et al., 2021; Qabany and Soga, 2014; Van Paassen et al., 2010; Li et al., 2024). During the Unconfined Compressive Strength (UCS) test, axial pressure is applied to the specimen without any confining pressure until failure occurs. The axial pressure recorded at the point of specimen failure represents the UCS of the specimen. Previous studies have reported that the produced $CaCO_3$ can fill soil pores and cement soil particles after EICP treatment, thereby enhancing the UCS of treated soil (DeJong et al., 2010; Yasuhara et al., 2012). A higher UCS indicates greater soil shear strength, which helps prevent slope failure during rainfall periods. There are many factors impacting the UCS of EICP-treated sand, such as the concentration of added Ca^{2+}, EICP treatment cycles, particle size distribution, and others. In previous studies, the UCS of EICP-treated sand ranged from 50 kPa to 1500 kPa, whereas untreated sand has no strength (Liu et al., 2023a; Liu et al., 2024).

The unconfined compressive strength (UCS) and corresponding calcium carbonate content of EICP-treated sand specimens were shown in Fig. 8(a). It is worth mentioning that, the sand specimens without adding Ca^{2+} had no strength, and thus, it is not depicted in Fig. 8(a). The UCS of sand specimens increased with the higher concentrations of added Ca^{2+} and treatment cycles, reaching the maximum of 306 kPa after four treatment cycles. Besides, the $CaCO_3$ generated in sand specimens basically correlated with UCS, indicating that the generated $CaCO_3$ could effectively cement sand particles and provide enough strength (Li et al., 2021). Fig. 8(a) also shows that the failure mode of the sand specimen. Different from the tensile splitting mode with a vertical crack through the whole specimen (Almajed et al., 2019; Liu et al., 2023a; Qabany and Soga, 2014), the failure mode in this study was shear failure accompanied by localized crushing failure in the bottom. The shear failure in this study indicates that the distribution of $CaCO_3$ was not uniform, which is possibly due to the high urease activity of sword bean urease. The same failure mode was confirmed by Zhang et al. (2023), who reported that sand specimen was tensile splitting failure when treated by low activity soybean urease (around 7.45 mmol/L/min), while shear failure treated with higher activity soybean urease (around 13.95 and 22.23 mmol/L/min). Besides, the localized crushing failure in the bottom may be caused by accumulated salted-out organic matter after four treatment cycles, resulting in the pore-clogging in the upper part of sand specimen and less $CaCO_3$ would form in the bottom part. Similar results were found by Liu et al. (2023a), who pointed out that the organic matter in urease solution can lead to surface clogging, and the corresponding failure mode would be localized crushing.

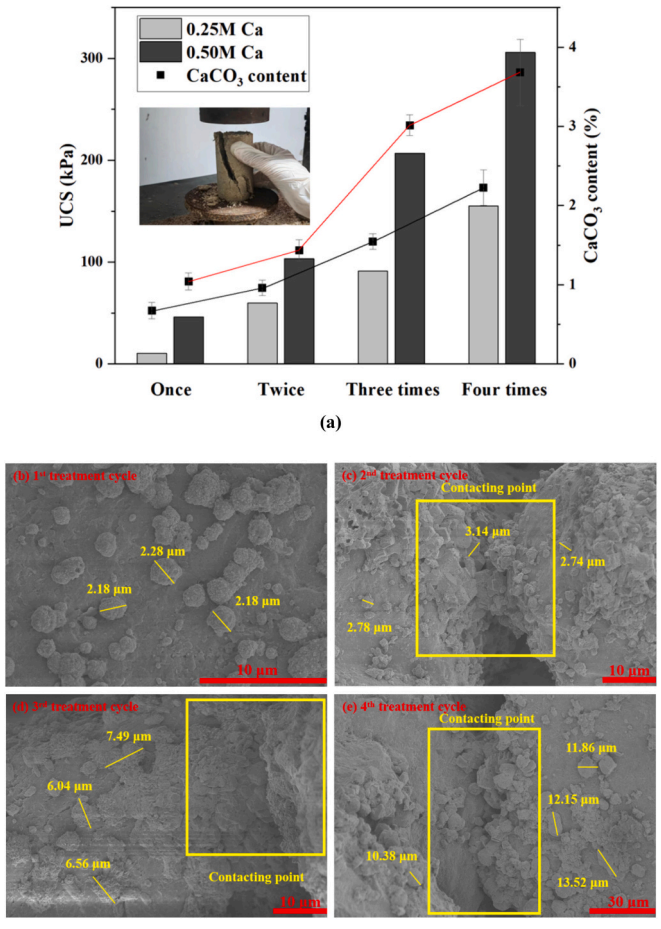

Fig. 8. UCS and microscale analysis of EICP-treated sand particles (a) Unconfined compressive stress, $CaCO_3$ content and failure mode; (b) SEM results after 1st treatment cycle; (c) SEM results after 2nd treatment cycle; (d) SEM results after 3rd treatment cycle; (e) SEM results after 4th treatment cycle.

3.3.2. Microscale analysis of treated sand

Fig. 8(b)–(e) shows the SEM results of sand specimens after 1st ~ 4th treatment cycles. Precipitate morphology can be summarized as spherical and rhombohedral, which may be due to the complex structure of bio-$CaCO_3$ combined with heavy metal carbonate and hydroxide. As the number of treatment cycles increased, the size of precipitate particles gradually increased, from 2.18 μm to 13.5 μm, and the number of precipitate particles also gradually increases. A large number of precipitate particles were formed at the contacting points between particles from 2nd to 4th treatment cycle, gradually bridging pores, thus forming effective crystals to cement sand particles. SEM results provide better explanations for UCS gradually increasing with the number of treatment cycles from a microscopic mechanism perspective.

3.4. Limitations and future work

This study investigated the effects of EICP on the efficacy of heavy metal immobilization (Zn^{2+}, Ni^{2+}, and Cr(VI)) and the unconfined compressive strength enhancement in contaminated sand. However, it is worth mentioning that the ammonia produced during EICP process poses a risk of secondary contamination to groundwater or environment. The ammonia/ammonium can lead to the eutrophication of water bodies, thus damaging the entire aquatic ecosystem (Li et al., 2020; Wang et al., 2020b). The next step for this study will be to develop some methods to remove the ammonia during the EICP process. Common methods for removing ammonia include air stripping, break-point chlorination, ion-exchange, and nitrification–denitrification (Değermenci et al., 2012; Jorgensen and Weatherley, 2003; Miladinovic and Weatherley, 2008; Pressley et al., 1972). In addition, some researchers have used EICP with a modified electrokinetic reactor containing a permeable reactive barrier (EK-PRB) to remove ammonia nitrogen (Wang et al., 2024b; Wang et al., 2023a). Specially, the struvite precipitation method was adopted into the EK-PRB. Struvite precipitates ($MgNH_4PO_4{\cdot}6H_2O$) could be formed by adding magnesium (Mg) and phosphate (P) to combine with NH_4^+, thereby achieving NH_4^+ recovery. The specific process was shown in Eq. (5). These methods could be employed as references to remove the ammonia nitrogen of this study, which necessitates further investigation.

$$Mg^{2+} + NH_4^+ + PO_4^{3-} + 6H_2O \rightarrow MgNH_4PO_4 \bullet 6H_2O \quad (5)$$

4. Conclusions

In this study, the immobilization heavy metals efficacy (Zn^{2+}, Ni^{2+}, and Cr(VI)) and strength enhancement of contaminated sand was

investigated by using EICP method with crude sword bean urease. Both liquid batch tests and sand specimen remediation experiments were conducted. Based on the results in the above experiments, the following conclusions can be drawn:

(a) The EICP method with crude sword bean urease can immobilize Zn^{2+}, Ni^{2+}, and Cr(VI) in liquid batch tests, with higher Ca^{2+} concentrations enhancing immobilization efficacy. In solutions with 0.5 mol/L Ca^{2+} added, the immobilization percentages are up to 99 % for Zn^{2+}, 40–50 % for Ni^{2+}, and 35–40 % for Cr(VI), respectively.
(b) The EICP method can effectively immobilize Zn^{2+}, Ni^{2+}, and Cr (VI) in contaminated sand, and the immobilization percentage increased with the addition of Ca^{2+} and treatment cycles. The final immobilization percentage of Zn^{2+}, Ni^{2+}, and Cr(VI) was up to 99.87–99.99 %, 83.43–86.38 %, and 73.43–75.18 %, respectively.
(c) After EICP treatment, the immobilization mechanism of heavy metals in both solution and sand can be considered as biomineralization, as well as adsorption and complexation by organic matter and $CaCO_3$.
(d) The strength of the EICP-treated contaminated sand specimens was significantly enhanced up to 306 kPa after four treatment cycles. The bio-precipitates were formed at the contacting points between sand particles, thus forming effective cementation. This indicates that EICP method holds the potential to improve the strength of heavy metal-contaminated sand.

CRediT authorship contribution statement

Yi Bian: Writing – original draft, Methodology, Investigation, Conceptualization. **Yanbo Chen:** Writing – review & editing, Methodology, Investigation. **Liangtong Zhan:** Writing – review & editing, Methodology, Conceptualization. **Haowen Guo:** Writing – review & editing, Methodology. **Han Ke:** Writing – review & editing, Methodology. **Yuze Wang:** Writing – review & editing, Methodology. **Qingyang Wang:** Methodology. **Yufeng Gao:** Writing – review & editing, Methodology. **Yunqi Gao:** Writing – review & editing, Methodology.

Declaration of competing interest

The authors declare that they have no known competing financial interests or personal relationships that could have appeared to influence the work reported in this paper.

Data availability

Data will be made available on request.

Acknowledgements

The authors would like to express their gratitude for the financial support provided by Key Research and Development Program of Zhejiang (No. 2022C03095), the National Natural Science Foundation of China (Grants 51988101 and 52208373), the Fundamental Research Funds for the Central Universities (No. 226202400057) and Hebei Natural Science Foundation (E2023201036).

Appendix A. Supplementary data

Supplementary data to this article can be found online at https://doi.org/10.1016/j.scitotenv.2024.174409.

References

Abdel-Gawwad, H.A., Saleh, A.A., Sikora, P., Elrahman, M.A., Mohammed, M.S., Hussein, H.S., et al., 2020. Biocarbonation: a novel method for synthesizing nano-zinc/zirconium carbonates and oxides. Arab. J. Chem. 13, 8092–8099.
Achal, V., Pan, X., Zhang, D., 2011. Remediation of copper-contaminated soil by Kocuria flava CR1, based on microbially induced calcite precipitation. Ecol. Eng. 37, 1601–1605.
Achal, V., Pan, X., Zhang, D., Fu, Q.-L., 2012. Bioremediation of Pb-contaminated soil based on microbially induced calcite precipitation. J. Microbiol. Biotechnol. 22 (2), 244–247.
Ahenkorah, I., Rahman, M.M., Karim, M.R., Teasdale, P.R., 2020. Optimization of enzyme induced carbonate precipitation (EICP) as a ground improvement technique. Geo-Congress 2020, 552–561.
Ahenkorah, I., Rahman, M.M., Karim, M.R., Beecham, S., Saint, C., 2021. A review of enzyme induced carbonate precipitation (EICP): the role of enzyme kinetics. Sustainable Chemistry 2, 92–114.
Ahmad, K., Bhatti, I.A., Muneer, M., Iqbal, M., Iqbal, Z., 2012. Removal of Heavy Metals (Zn, Cr, Pb, Cd, Cu and Fe) in Aqueous Media by Calcium Carbonate as an Adsorbent.
Akbarpour, F., Gitipour, S., Baghdadi, M., Mehrdadi, N., 2021. Correlation between chemical fractionation of heavy metals and their toxicity in the contaminated soils. Environ. Earth Sci. 80.
Almajed, A., Khodadadi Tirkolaei, H., Kavazanjian, E., 2018. Baseline investigation on enzyme-induced calcium carbonate precipitation. J. Geotech. Geoenviron. Eng. 144.
Almajed, A., Tirkolaei, H.K., Kavazanjian Jr., E., Hamdan, N., 2019. Enzyme induced biocementated sand with high strength at low carbonate content. Sci. Rep. 9, 1135.
ASTM I, 2010. Standard Test Method for Unconfined Compressive Strength of Cohesive Soil. ASTM. 2010. ASTM D2166/2166M-13. ASTM, West Conshohocken, PA.
Blundell, T., Jenkins, J., 1977. The binding of heavy metals to proteins. Chem. Soc. Rev. 6, 139–171.
Böhlke, J.K., Smith, R.L., Miller, D.N., 2006. Ammonium transport and reaction in contaminated groundwater: application of isotope tracers and isotope fractionation studies. Water Resour. Res. 42.
Chang, I.-S., Chung, C.-M., 2000. Pollution prevention for manufacturing of ammonium chloride - an ecperimental study of wastewater recycling. Desalination 127, 145–153.
Chen, Wright J.V., Conca, J.L., Peurrung, L.M., 1997. Effects of pH on heavy metal sorption on mineral apatite. Environ. Sci. Technol. 31, 624–631.
Chen, Y., Gao, Y., Guo, H., 2021a. Bio-improved hydraulic properties of sand treated by soybean urease induced carbonate precipitation and its application Part 2: Sand-geotextile capillary barrier effect. Transp. Geotech. 27, 100484.
Chen, Y., Gao, Y., Ng, C.W.W., Guo, H., 2021b. Bio-improved hydraulic properties of sand treated by soybean urease induced carbonate precipitation and its application Part 1: Water retention ability. Transp. Geotech. 27, 100489.
Chen, Y., Liu, B., Bian, Y., et al., 2024. Effects of soybean urease induced carbonate precipitation on the seed emergence and seedling growth of *Caragana korshinskii Kom* and its application in wind erosion control. Plant Soil. https://doi.org/10.1007/s11104-024-06758-9.
Choi, M., Jang, J., 2008. Heavy metal ion adsorption onto polypyrrole-impregnated porous carbon. J. Colloid Interface Sci. 325, 287–289.
Cui, M.-J., Lai, H.-J., Wu, S.-F., Chu, J., 2022. Comparison of soil improvement methods using crude soybean enzyme, bacterial enzyme or bacteria-induced carbonate precipitation. Géotechnique 1–9.
Cui, M.J., Chu, J., Lai, H.J., 2024. Optimization of one-phase-low-pH enzyme-induced carbonate precipitation method for soil improvement. Acta Geotech 19, 1611–1625. https://doi.org/10.1007/s11440-023-02175-x.
Da Silva, J.F., Williams, R.J.P., 2001. The Biological Chemistry of the Elements: The Inorganic Chemistry of Life. Oxford University Press.
Daneshvar, N., Salari, D., Aber, S., 2002. Chromium adsorption and Cr(VI) reduction to trivalent chromium in aqueous solutions by soya cake. J. Hazard. Mater. 94, 49–61.
Deak, N.A., Murphy, P.A., Johnson, L.A., 2006. Effects of NaCl concentration on salting-in and dilution during salting-out on soy protein fractionation. J. Food Sci. 71, C247–C254.
Değermenci, N., Ata, O.N., Yildız, E., 2012. Ammonia removal by air stripping in a semi-batch jet loop reactor. J. Ind. Eng. Chem. 18, 399–404.
DeJong, J.T., Mortensen, B.M., Martinez, B.C., Nelson, D.C., 2010. Bio-mediated soil improvement. Ecol. Eng. 36, 197–210.
Devi, P., Saroha, A.K., 2014. Risk analysis of pyrolyzed biochar made from paper mill effluent treatment plant sludge for bioavailability and eco-toxicity of heavy metals. Bioresour. Technol. 162, 308–315.
Deze, E.G., Papageorgiou, S.K., Favvas, E.P., Katsaros, F.K., 2012. Porous alginate aerogel beads for effective and rapid heavy metal sorption from aqueous solutions: effect of porosity in Cu2+ and Cd2+ ion sorption. Chem. Eng. J. 209, 537–546.
Dhami, N.K., Quirin, M.E.C., Mukherjee, A., 2017. Carbonate biomineralization and heavy metal remediation by calcifying fungi isolated from karstic caves. Ecol. Eng. 103, 106–117.
Dinesh, R., Ramanathan, G., Singh, H., 1995. Influence of chloride and sulphate ions on soil enzymes. J. Agron. Crop Sci. 175, 129–133.
Erickson, H.P., 2009. Size and Shape of Protein Molecules at the Nanometer Level Determined by Sedimentation, Gel Filtration, and Electron Microscopy. Biol. Proced. Online 11, 32. https://doi.org/10.1007/s12575-009-9008-x.
Feng, S.-J., Chang, J.-Y., Shi, H., Zheng, Q.-T., Guo, X.-Y., Zhang, X.-L., 2019. Failure of an unfilled landfill cell due to an adjacent steep slope and a high groundwater level: a case study. Eng. Geol. 262, 105320.

Freij, S.J., Godelitsas, A., Putnis, A., 2005. Crystal growth and dissolution processes at the calcite–water interface in the presence of zinc ions. J. Cryst. Growth 273, 535–545.
Fu, F., Wang, Q., 2011. Removal of heavy metal ions from wastewaters: a review. J. Environ. Manag. 92, 407–418.
Gao, Y., He, J., Tang, X., Chu, J., 2019. Calcium carbonate precipitation catalyzed by soybean urease as an improvement method for fine-grained soil. Soils Found. 59, 1631–1637.
Gao, Y.-f., Meng, H., He, J., Qi, Y.-s., Hang, L., 2020. Field trial on use of soybean crude extract for carbonate precipitation and wind erosion control of sandy soil. J. Cent. South Univ. 27, 3320–3333.
Godelitsas, A., Astilleros, J.M., Hallam, K., Harissopoulos, S., Putnis, A., 2003. Interaction of calcium carbonates with lead in aqueous solutions. Environ. Sci. Technol. 37, 3351–3360.
Guo, H., Chen, Y., Zhang, Q., Lu, H., 2023. Effects of biochar on plant growth and hydro-chemical properties of recycled concrete aggregate. Sci. Total Environ. 882, 163557.
Han, Z.Y., Xu, M., Liu, G., Cheng, C., 2015. Pollutant identification and quality assessment of groundwater near municipal solid waste landfills in China. China Environ. Sci. 35, 2843–2852.
Han, Z., Ma, H., Shi, G., He, L., Wei, L., Shi, Q., 2016. A review of groundwater contamination near municipal solid waste landfill sites in China. Sci. Total Environ. 569-570, 1255–1264.
Hendry, M.T., 2018. Shear strength. In: Bobrowsky, P.T., Marker, B. (Eds.), Encyclopedia of Engineering Geology. Springer International Publishing, Cham, pp. 831–833.
Hidri, R., Mahmoud, O.M.-B., Zorrig, W., Mahmoudi, H., Smaoui, A., Abdelly, C., et al., 2022. Plant growth-promoting Rhizobacteria alleviate high salinity impact on the halophyte Suaeda fruticosa by modulating antioxidant defense and soil biological activity. Frontiers. Plant Sci. 13.
Horne, D.S., 1998. Casein interactions: casting light on the black boxes, the structure in dairy products. Int. Dairy J. 8, 171–177.
Hossain, M., Islam, M.A., Badhon, F., Imtiaz, T., 2021. Properties and Behavior of Soil - Online Lab Manual.
Hu, W., Peng, C., Lv, M., Li, X., Zhang, Y., Chen, N., et al., 2011. Protein corona-mediated mitigation of cytotoxicity of graphene oxide. ACS Nano 5, 3693–3700.
Hu, L., Wang, H., Xu, P., Zhang, Y., 2021a. Biomineralization of hypersaline produced water using microbially induced calcite precipitation. Water Res. 190, 116753.
Hu, W., Cheng, W.-C., Wen, S., Yuan, K., 2021b. Revealing the enhancement and degradation mechanisms affecting the performance of carbonate precipitation in EICP process. Front. Bioeng. Biotechnol. 9.
Hua, R., Li, Z., 2014. Sulfhydryl functionalized hydrogel with magnetism: synthesis, characterization, and adsorption behavior study for heavy metal removal. Chem. Eng. J. 249, 189–200.
Huang, Y., Fan, G., 2016. Engineering geological analysis of municipal solid waste landfill stability. Nat. Hazards 84, 93–107.
Intawongse, M., Dean, J.R., 2006. Uptake of heavy metals by vegetable plants grown on contaminated soil and their bioavailability in the human gastrointestinal tract. Food Addit. Contam. 23, 36–48.
Jiménez-Rodríguez, A.M., Durán-Barrantes, M.M., Borja, R., Sánchez, E., Colmenarejo, M.F., Raposo, F., 2009. Heavy metals removal from acid mine drainage water using biogenic hydrogen sulphide and effluent from anaerobic treatment: effect of pH. J. Hazard. Mater. 165, 759–765.
Jorgensen, T.C., Weatherley, L.R., 2003. Ammonia removal from wastewater by ion exchange in the presence of organic contaminants. Water Res. 37, 1723–1728.
Kang, C.-H., Oh, S.J., Shin, Y., Han, S.-H., Nam, I.-H., So, J.-S., 2015. Bioremediation of lead by ureolytic bacteria isolated from soil at abandoned metal mines in South Korea. Ecol. Eng. 74, 402–407.
Kang, C.-H., Kwon, Y.-J., So, J.-S., 2016. Bioremediation of heavy metals by using bacterial mixtures. Ecol. Eng. 89, 64–69.
Karnchanawong, S., Limpiteeprakan, P., 2009. Evaluation of heavy metal leaching from spent household batteries disposed in municipal solid waste. Waste Manag. 29, 550–558.
Kasassi, A., Rakimbei, P., Karagiannidis, A., Zabaniotou, A., Tsiouvaras, K., Nastis, A., et al., 2008. Soil contamination by heavy metals: measurements from a closed unlined landfill. Bioresour. Technol. 99, 8578–8584.
Kavazanjian, E., Hamdan, N., 2015. Enzyme induced carbonate precipitation (EICP) columns for ground improvement. IFCEE 2015, 2252–2261.
Khan, S., Naushad, M., Lima, E.C., Zhang, S., Shaheen, S.M., Rinklebe, J., 2021. Global soil pollution by toxic elements: current status and future perspectives on the risk assessment and remediation strategies – a review. J. Hazard. Mater. 417, 126039.
Khodadadi Tirkolaei, H., Javadi, N., Krishnan, V., Hamdan, N., Kavazanjian, E., 2020. Crude urease extract for biocementation. J. Mater. Civ. Eng. 32.
Khodadadi, T.H., Kavazanjian, E., Paassen, Lv, DeJong, J., 2017. Bio-grout materials: a review. Grouting 2017, 1–12.
Knape, M.J., Ahuja, L.G., Bertinetti, D., Burghardt, N.C.G., Zimmermann, B., Taylor, S.S., et al., 2015. Divalent metal ions Mg2+ and Ca2+ have distinct effects on protein kinase A activity and regulation. ACS Chem. Biol. 10, 2303–2315.
Koerner, Robert M., Soong, T.-Y., 2012. Stability Assessment of Ten Large Landfill Failures. Advances in Transportation and Geoenvironmental Systems Using Geosynthetics, pp. 1–38.
Krajewska, B., 2016. A combined temperature-pH study of urease kinetics. Assigning pKa values to ionizable groups of the active site involved in the catalytic reaction. J. Mol. Catal. B Enzym. 124, 70–76.
Krajewska, B., 2018. Urease-aided calcium carbonate mineralization for engineering applications: a review. J. Adv. Res. 13, 59–67.
Kumpiene, J., Lagerkvist, A., Maurice, C., 2008. Stabilization of As, Cr, Cu, Pb and Zn in soil using amendments – a review. Waste Manag. 28, 215–225.
Lai, H.-J., Cui, M.-J., Chu, J., 2023. Effect of pH on soil improvement using one-phase-low-pH MICP or EICP biocementation method. Acta Geotech. 18, 3259–3272.
Lai, H., Ding, X., Cui, M., Zheng, J., Chu, J., Chen, Z., 2024. Factors affecting the effectiveness of biocementation of soil. Biogeotechnics 3, 100087.
Lakshtanov, L.Z., Stipp, S.L.S., 2007. Experimental study of nickel(II) interaction with calcite: adsorption and coprecipitation. Geochim. Cosmochim. Acta 71, 3686–3697.
Lee, J.-J., Yang, S.-Y., Park, J., Ferrell, J.E., Shin, D.-H., Lee, K.-J., 2017. Calcium ion induced structural changes promote dimerization of secretagogin, which is required for its insulin secretory function. Sci. Rep. 7, 6976.
Li Q, Liu Z, Wang C, Zhao Y, Che R. Doping of Ni and Zn elements in MnCO3: high-power anode material for lithium–ion batteries. Small 2017; 14.
Li, Y., Li, Y., Guo, Z., Xu, Q., 2023. Durability of MICP-reinforced calcareous sand in marine environments: laboratory and field experimental study. Biogeotechnics 3, 100018.
Li, Y., Guo, Z., Wang, L., Zhu, Y., Rui, S., 2024. Field implementation to resist coastal erosion of sandy slope by eco-friendly methods. Coast. Eng. 189, 104489.
Li, Q., Liu, D., Chen, C., Shao, Z., Wang, H., Liu, J., et al., 2019. Experimental and geochemical simulation of nickel carbonate mineral precipitation by carbonate-laden ureolytic fungal culture supernatants. Environ. Sci. Nano 6, 1866–1875.
Li, D., Xu, X., Li, Z., Wang, T., Wang, C., 2020. Detection methods of ammonia nitrogen in water: a review. TrAC Trends Anal. Chem. 127, 115890.
Li, Y., Guo, Z., Wang, L., Ye, Z., Shen, C., Zhou, W., 2021. Interface shear behavior between MICP-treated calcareous sand and steel. J. Mater. Civ. Eng. 33, 04020455.
Li, W., Zhang, Y., Achal, V., 2022. Mechanisms of cadmium retention on enzyme-induced carbonate precipitation (EICP) of Ca/Mg: nucleation, chemisorption, and co-precipitation. J. Environ. Chem. Eng. 10, 107507.
Liang, W., Bai, J., Li, Z., Meng, Y., Liu, K., Li, L., 2022. Crystal growth, structure and thermal properties of anhydrous zinc carbonate (ZnCO3). J. Alloys Compd. 898, 162916.
Liu, H.-H., Sang, S.-X., 2010. Study on the law of heavy metal leaching in municipal solid waste landfill. Environ. Monit. Assess. 165, 349–363.
Liu, Z., Teng, F., 2018. Understanding the correlation of crystal atoms with photochemistry property: Zn5(OH)6(CO3)2vs. ZnCO3. ChemistrySelect 3, 8886–8894.
Liu, D., Li, Z., Li, W., Zhong, Z., Xu, J., Ren, J., et al., 2013. Adsorption behavior of heavy metal ions from aqueous solution by soy protein hollow microspheres. Ind. Eng. Chem. Res. 52, 11036–11044.
Liu, P., Zhang, Y., Tang, Q., Shi, S., 2021. Bioremediation of metal-contaminated soils by microbially-induced carbonate precipitation and its effects on ecotoxicity and long-term stability. Biochem. Eng. J. 166, 107856.
Liu, L., Chen, Y., Gao, Y., Liu, B., Zhou, Y., Li, C., 2023a. Effect of urease enrichment degree of multiple sources of urease on bio-cementation efficacy via enzyme-induced carbonate precipitation. Can. Geotech. J. 0: null.
Liu, Y., Lu, S., Meng, J., Xiang, H., Korma, S.A., Cacciotti, I., et al., 2023b. Complexation between egg yolk protein hydrolysate, phytic acid and calcium ion: binding mechanisms and influence on protein digestibility and calcium uptake. LWT 184, 114986.
Liu, L., Gao, Y., Meng, H., Pan, Q., Wang, Z., Zhou, Y., et al., 2024. Pore-scale, mechanical, and hydraulic properties of EICP-treated sand using crude legume ureases with different protein contents. Acta Geotech.
Maeda, M., Okada, K., Tsukamoto, Y., Wakabayashi, K., Ito, K., 1990. Complex formation of calcium(II) with amino acids under physiological conditions. J. Chem. Soc. Dalton Trans. 2337–2339.
Mao, X., Xiong, L., Hu, X., Yan, Z., Wang, L., Xu, G., 2018. Remediation of ammonia-contaminated groundwater in landfill sites with electrochemical reactive barriers: a bench scale study. Waste Manag. 78, 69–78.
Martin, K., Tirkolaei, H.K., Kavazanjian, E., 2021. Enhancing the strength of granular material with a modified enzyme-induced carbonate precipitation (EICP) treatment solution. Constr. Build. Mater. 271, 121529.
Matsumoto, M., Fukunaga, T., Onoe, K., 2010. Polymorph control of calcium carbonate by reactive crystallization using microbubble technique. Chem. Eng. Res. Des. 88, 1624–1630.
Meng, H., Shu, S., Gao, Y., Yan, B., He, J., 2021. Multiple-phase enzyme-induced carbonate precipitation (EICP) method for soil improvement. Eng. Geol. 294, 106374.
Miao, L., Wang, H., Sun, X., Wu, L., Fan, G., 2024. Effect analysis of biomineralization for solidifying desert sands. Biogeotechnics 2, 100065.
Miladinovic, N., Weatherley, L.R., 2008. Intensification of ammonia removal in a combined ion-exchange and nitrification column. Chem. Eng. J. 135, 15–24.
Moghal, A.A.B., Lateef, M.A., Mohammed, S.A.S., Lemboye, K., C. S. Chittoori, B., Almajed, A., 2020. Efficacy of enzymatically induced calcium carbonate precipitation in the retention of heavy metal ions. Sustainability 12, 7019.
Moghal, A.A.B., Rasheed, R.M., Mohammed, S.A.S., 2023. Sorptive and desorptive response of divalent heavy metal ions from EICP-treated plastic fines. Indian Geotech. J. 53, 315–333.
Nam, I.-H., Chon, C.-M., Jung, K.-Y., Choi, S.-G., Choi, H., Park, S.-S., 2014. Calcite precipitation by ureolytic plant (Canavalia ensiformis) extracts as effective biomaterials. KSCE J. Civ. Eng. 19, 1620–1625.
Nam, I.-H., Roh, S.-B., Park, M.-J., Chon, C.-M., Kim, J.-G., Jeong, S.-W., et al., 2016. Immobilization of heavy metal contaminated mine wastes using Canavalia ensiformis extract. Catena 136, 53–58.
Nkutha, C.S., Naidoo, E.B., Shooto, N.D., 2021. Adsorptive studies of toxic metal ions of Cr(VI) and Pb(II) from synthetic wastewater by pristine and calcined coral limestones. South African Journal of Chemical Engineering 36, 43–57.

Palansooriya, K.N., Shaheen, S.M., Chen, S.S., Tsang, D.C.W., Hashimoto, Y., Hou, D., et al., 2020. Soil amendments for immobilization of potentially toxic elements in contaminated soils: a critical review. Environ. Int. 134, 105046.
Ping, Z., Zou, B., Li, N., Li, Z., 2009. Heavy metal contamination in soils and food crops around Dabaoshan mine in Guangdong, China: implication for human health. Environ. Geochem. Health 31, 707–715.
Pressley, T.A., Bishop, D.F., Roan, S.G., 1972. Ammonia-nitrogen removal by breakpoint chlorination. Environ. Sci. Technol. 6, 622–628.
Pruvot, C., Douay, F., Hervé, F., Waterlot, C., 2006. Heavy metals in soil, crops and grass as a source of human exposure in the former mining areas (6 pp). J. Soils Sediments 6, 215–220.
Qabany, A.A., Soga, K., 2014. Effect of chemical treatment used in MICP on engineering properties of cemented soils. In: Bio- and Chemo-mechanical Processes in Geotechnical Engineering: Géotechnique Symposium in Print 2013. ICE Publishing, pp. 107–115.
Qi, Y., Gao, Y., Meng, H., He, J., Liu, Y., 2022. Biocementation via soybean-urease induced carbonate precipitation using carbide slag powder derived soluble calcium. Geomechanics and Engineering 29, 79–90.
Qu, Y., Teichert, B.M.A., Birgel, D., Goedert, J.L., Peckmann, J., 2017. The prominent role of bacterial sulfate reduction in the formation of glendonite: a case study from Paleogene marine strata of western Washington State. Facies 63, 1–16.
Rosado-Mendoza, M., Oliva-Avilés, A.I., Oliva, A.I., 2018. Preferential regions of growth of chemical bath deposited ZnO and Zn(OH)2 thin films at room conditions. Thin Solid Films 645, 231–240.
Salleh, N.F.D.M., Hamid, K.H.K., 2013. Effect of rainfall on aged landfill leachate constituents. IEEE Business Engineering and Industrial Applications Colloquium (BEIAC) 2013, 257–261.
Sánchez-Pastor, N., Gigler, A.M., Cruz, J.A., Park, S.-H., Jordan, G., Fernández-Díaz, L., 2011. Growth of calcium carbonate in the presence of Cr(VI). Cryst. Growth Des. 11, 3081–3089.
Sengor, S., Barua, S., Gikas, P., Ginn, T., Peyton, B., Sani, R., et al., 2009. Influence of heavy metals on microbial growth kinetics including lag time: mathematical modeling and experimental verification. Environmental Toxicology and Chemistry/SETAC 28, 2020–2029.
Sharma, M., Satyam, N., Reddy, K.R., Chrysochoou, M., 2022. Multiple heavy metal immobilization and strength improvement of contaminated soil using bio-mediated calcite precipitation technique. Environ. Sci. Pollut. Res. Int. 29, 51827–51846.
Sheng, X., Chen, S., Zhao, Z., Li, L., Zou, Y., Shi, H., et al., 2023. Rationally designed calcium carbonate multifunctional trap for contaminants adsorption. Sci. Total Environ. 903, 166142.
Shi, H.-S., Kan, L.-L., 2009. Leaching behavior of heavy metals from municipal solid wastes incineration (MSWI) fly ash used in concrete. J. Hazard. Mater. 164, 750–754.
Smith, S., Peterson, P., Kwan, K., 1989. Chromium accumulation, transport and toxicity in plants. Toxicol. Environ. Chem. 24, 241–251.
Song, X., Cao, Y., Bu, X., Luo, X., 2021. Porous vaterite and cubic calcite aggregated calcium carbonate obtained from steamed ammonia liquid waste for Cu2+ heavy metal ions removal by adsorption process. Appl. Surf. Sci. 536, 147958.
Song, H., Kumar, A., Ding, Y., Wang, J., Zhang, Y., 2022. Removal of Cd2+ from wastewater by microorganism induced carbonate precipitation (MICP): an economic bioremediation approach. Sep. Purif. Technol. 297, 121540.
Stark Timothy, D., Eid Hisham, T., Evans, W.D., Sherry, Paul E., 2000. Municipal solid waste slope failure. II: stability analyses. J. Geotech. Geoenviron. Eng. 126, 408–419.
Tang, Q.G., Meng, J.P., Liang, J.S., Nie, L., Li, Y.X., 2010. Effects of copper based alloys on the nucleation and growth of calcium carbonate scale. J. Alloys Compd. 491, 242–247.
Tessier, A., Campbell, P.G.C., Bisson, M., 1979. Sequential extraction procedure for the speciation of particulate trace metals. Anal. Chem. 51, 844–851.
Tyagi, B., Gupta, B., Thakur, I.S., 2020. Biosorption of Cr (VI) from aqueous solution by extracellular polymeric substances (EPS) produced by Parapedobacter sp. ISTM3 strain isolated from Mawsmai cave, Meghalaya, India. Environ. Res. 191, 110064.
Vakili, M., Rafatullah, M., Yuan, J., Zwain, H.M., Mojiri, A., Gholami, Z., et al., 2021. Nickel ion removal from aqueous solutions through the adsorption process: a review. Rev. Chem. Eng. 37, 755–778.
Van Paassen, L.A., Daza, C.M., Staal, M., Sorokin, D.Y., van der Zon, W., van Loosdrecht, M.C., 2010. Potential soil reinforcement by biological denitrification. Ecol. Eng. 36, 168–175.
Vu, X.H., Nguyen, L.H., Van, H.T., Nguyen, D.V., Nguyen, T.H., Nguyen, Q.T., et al., 2019. Adsorption of chromium(VI) onto freshwater snail shell-derived biosorbent from aqueous solutions: equilibrium, kinetics, and thermodynamics. J. Chemother. 2019, 1–11.
Wada, N., Yamashita, K., Umegaki, T., 1995. Effects of divalent cations upon nucleation, growth and transformation of calcium carbonate polymorphs under conditions of double diffusion. J. Cryst. Growth 148, 297–304.
Wang, P., Shen, T., Li, X., Tang, Y., Li, Y., 2020a. Magnetic Mesoporous Calcium Carbonate-based Nanocomposites for the Removal of Toxic Pb(II) and Cd(II) Ions from Water.
Wang, X., Li, J., Chen, J., Cui, L., Li, W., Gao, X., et al., 2020b. Water quality criteria of total ammonia nitrogen (TAN) and un-ionized ammonia (NH3-N) and their ecological risk in the Liao River. China. Chemosphere 243, 125328.
Wang, L., Cheng, W.C., Xue, Z.-F., Zhang, B., Lv, X., 2022. Immobilizing of lead and copper using chitosan-assisted enzyme-induced carbonate precipitation. Environ. Pollut. 319, 120947.
Wang, L., Cheng, W.-C., Xue, Z.-F., Xie, Y.-X., Lv, X.-J., 2023a. Feasibility study of applying electrokinetic technology coupled with enzyme-induced carbonate precipitation treatment to Cu- and Pb-contaminated loess remediation. J. Clean. Prod. 401, 136734.
Wang, L., Cheng, W.-C., Xue, Z.-F., Xie, Y.-X., Lv, X.-J., 2023b. Study on Cu- and Pb-contaminated loess remediation using electrokinetic technology coupled with biological permeable reactive barrier. J. Environ. Manag. 348, 119348.
Wang, L., Cheng, W.-C., Xue, Z.-F., Zhang, B., Lv, X.-J., 2023c. Immobilizing of lead and copper using chitosan-assisted enzyme-induced carbonate precipitation. Environ. Pollut. 319, 120947.
Wang, F., Li, W., Wang, H., Hu, Y., Cheng, H., 2024a. The leaching behavior of heavy metal from contaminated mining soil: the effect of rainfall conditions and the impact on surrounding agricultural lands. Sci. Total Environ. 914, 169877.
Wang, Y.K., Chen, H., Chen, Y.B., Jiao, M.J., Fan, Z.Y., 2024. Experimental study on macro-micro effectiveness of Yellow River silt solidified by using soybean-induced carbonate precipitation (SICP) technology. Mar. Georesources Geotechnol. 1–11. https://doi.org/10.1080/1064119X.2024.2318395.
Wang, L., Cheng, W.-C., Xue, Z.-F., Rahman, M.M., Xie, Y.-X., 2024b. Struvite and ethylenediaminedisuccinic acid (EDDS) enhance electrokinetic-biological permeable reactive barrier removal of copper and lead from contaminated loess. J. Environ. Manag. 360, 121100.
Whiffin, V.S., 2004. In: Cord-Ruwisch, R. (Ed.), Microbial CaCO3 Precipitation for the Production of Biocement.
Whiffin, V.S., van Paassen, L.A., Harkes, M.P., 2007. Microbial carbonate precipitation as a soil improvement technique. Geomicrobiol J. 24, 417–423.
Wickramarachchi, P., Kawamoto, K., Hamamoto, S., Nagamori, M., Moldrup, P., Komatsu, T., 2011. Effects of dry bulk density and particle size fraction on gas transport parameters in variably saturated landfill cover soil. Waste Manag. 31, 2464–2472.
Xiao, Y., He, X., Evans, T.M., Stuedlein, A.W., Liu, H., 2019. Unconfined compressive and splitting tensile strength of basalt fiber–reinforced biocemented sand. J. Geotech. Geoenviron. Eng. 145, 04019048.
Xiao, Y., Xiao, W., Wu, H., Zhao, H., Liu, H., 2023. Particle size effect on unconfined compressive strength of biotreated sand. Transportation Geotechnics 42, 101092.
Xie, D., Zhang, R., Wang, J., 2023. The influence of environmental factors and precipitation precursors on enzyme-induced carbonate precipitation (EICP) process and its application on modification of recycled concrete aggregates. J. Clean. Prod. 395, 136444.
Xie, Y.-X., Cheng, W.-C., Xue, Z.-F., Rahman, M.M., Wang, L., 2024. Deterioration phenomenon of Pb-contaminated aqueous solution remediation and enhancement mechanism of nano-hydroxyapatite-assisted biomineralization. J. Hazard. Mater. 470, 134210.
Xu, L., Su, J., Huang, T., Li, G., Ali, A., Shi, J., 2021. Simultaneous removal of nitrate and diethyl phthalate using a novel sponge–based biocarrier combined modified walnut shell biochar with Fe3O4 in the immobilized bioreactor. J. Hazard. Mater. 414, 125578.
Yang, X., Wan, Y., Zheng, Y., He, F., Yu, Z., Huang, J., et al., 2019. Surface functional groups of carbon-based adsorbents and their roles in the removal of heavy metals from aqueous solutions: a critical review. Chem. Eng. J. 366, 608–621.
Yao, D., Wu, J., Wang, G., Wang, P., Zheng, J.-J., Yan, J., et al., 2021. Effect of wool fiber addition on the reinforcement of loose sands by microbially induced carbonate precipitation (MICP): mechanical property and underlying mechanism. Acta Geotech. 16, 1401–1416.
Yasuhara, H., Neupane, D., Hayashi, K., Okamura, M., 2012. Experiments and predictions of physical properties of sand cemented by enzymatically-induced carbonate precipitation. Soils Found. 52, 539–549.
Yu, L., Batlle, F., 2011. A hybrid method for quasi-three-dimensional slope stability analysis in a municipal solid waste landfill. Waste Manag. 31, 2484–2496.
Yuan, H., Ren, G., Liu, K., Zheng, W., Zhao, Z., 2020. Experimental study of EICP combined with organic materials for silt improvement in the Yellow River flood area. Appl. Sci. 10, 7678.
Zeng, G., Qiao, S., Wang, X., Sheng, M., Wei, M., Chen, Q., et al., 2021. Immobilization of cadmium by Burkholderia sp. QY14 through modified microbially induced phosphate precipitation. J. Hazard. Mater. 412, 125156.
Zhan, L., Wang, J., Liang, T., Chen, Y., Wang, S., Lou, H., Zhang, H., 2023. Aggregation and dehydration of excavated soft clay and use for subgrade engineering–Part 1 A laboratory study. Transp. Geotech. 38, 100914.
Zhang, H., He, P.-J., Shao, L.-M., Li, X.-J., 2008. Leaching behavior of heavy metals from municipal solid waste incineration bottom ash and its geochemical modeling. J. Mater. Cycles Waste Manage. 10, 7–13.
Zhang, C.-l., Feng, J.-j., Zhao, T.-n., Rong, L.-m., 2017a. Physical, chemical, and engineering properties of landfill stabilized waste. Land Degrad. Dev. 28, 1113–1121.
Zhang, C., Zhu, X., Wu, L., Li, Q., Liu, J., Qian, G., 2017b. Calcium and organic matter removal by carbonation process with waste incineration flue gas towards improvement of leachate biotreatment performance. Bioresour. Technol. 240, 165–170.
Zhang, G., Qin, P., Nasser, R., Li, S., Chen, P., Song, J., 2020. Synthesis of Co(CO3)0.5(OH)/Ni2(CO3)(OH)2 nanobelts and their application in flexible all-solid-state asymmetric supercapacitor. Chem. Eng. J. 387, 124029.
Zhang, M., Shen, H., Qian, Z., Liu, H., Tian, D., Wang, X., 2022. Dual-purpose applications of magnetic phase-change microcapsules with crystalline-phase-tunable CaCO3 shell for waste heat recovery and heavy metal ion removal. Journal of Energy Storage 55, 105672.
Zhang, J., Yin, Y., Shi, W., Bian, H., Shi, L., Wu, L., et al., 2023. Strength and uniformity of EICP-treated sand under multi-factor coupling effects. Biogeotechnics 1, 100007.

Zhao, Q., Li, L., Li, C., Li, M., Amini, F., Zhang, H., 2014. Factors affecting improvement of engineering properties of MICP-treated soil catalyzed by bacteria and urease. J. Mater. Civ. Eng. 26, 04014094.
Zheng, K., Chen, P., Qiu, Y., Guo, Q., Chen, Y., Yuan, M., et al., 2022. Physicochemical properties and reuse of municipal solid waste fine fraction: case of an aged landfill site in Zhejiang Province. China Environ. Sci. 42, 3254–3264.
Zhou, Q., Liu, Y., Li, T., Zhao, H., Alessi, D.S., Liu, W., et al., 2020. Cadmium adsorption to clay-microbe aggregates: implications for marine heavy metals cycling. Geochim. Cosmochim. Acta 290, 124–136.